Waveforms MOdels for Machine Type CommuNication inteGrating 5G Networks (WONG5) Document Number D3.1

Hmaied Shaiek, Daniel Roviras, Yahia Medjahdi, Rafik Zayani, Mouna Ben Mabrouk, Yves Louët

▶ **To cite this version:**

Hmaied Shaiek, Daniel Roviras, Yahia Medjahdi, Rafik Zayani, Mouna Ben Mabrouk, et al.. Waveforms MOdels for Machine Type CommuNication inteGrating 5G Networks (WONG5) Document Number D3.1. [Research Report] Conservatoire national des arts et métiers - CNAM. 2017. hal-02456411

HAL Id: hal-02456411
https://cnam.hal.science/hal-02456411

Submitted on 4 Feb 2020

HAL is a multi-disciplinary open access archive for the deposit and dissemination of scientific research documents, whether they are published or not. The documents may come from teaching and research institutions in France or abroad, or from public or private research centers.

L'archive ouverte pluridisciplinaire **HAL**, est destinée au dépôt et à la diffusion de documents scientifiques de niveau recherche, publiés ou non, émanant des établissements d'enseignement et de recherche français ou étrangers, des laboratoires publics ou privés.

Waveforms MOdels for Machine Type CommuNication inteGrating 5G Networks

(WONG5)

Document Number D3.1

Performance of the candidate waveforms in the presence of power amplifier

Contractual date of delivery:	12/04/2017
Project Number and Acronym:	ANR-15-CE25-0005, WONG5
Editor:	CNAM
Authors:	Hmaied SHAIEK, Daniel ROVIRAS, Yahia MEDJAHDI, Rafik ZAYANI, Mouna BEN MABROUK, Yves LOUET.
Participants:	CNAM, CS
Workpackage:	WP3
Security:	PU
Nature:	Report
Version:	1.1
Total Number of Pages:	52

Abstract:

Multicarrier modulated signals suffer from high peak to average power ratio (PAPR), making them very sensitive to High Power Amplifiers (HPA) non-linearity. All waveforms studied in D2.1 will be sensitive to non-linear amplification. This sensitivity can be characterized in terms of Out of Band (OOB) or spectral regrowth and In-band distortion characterizing the errors over the transmitted data symbols. For OOB, the spectral regrowth must be kept under a certain level characterized by transmission spectral masks. Indeed, most of post OFDM waveforms have been proposed to have better frequency localization than classical CP-OFDM. The spectral effect of non-linear (NL) HPA has to be carefully studied and mitigated, if needed, for these waveforms. The second drawback of a NL HPA is related to the in-band non-linear noise and can be characterized in terms of Bit Error Rate (BER) or Error Vector Magnitude (EVM) degradation.

Keywords: Power amplifier models, IBO, PAPR, OOB, Spectral regrowth.

Document Revision History

Version	Date	Author	Summary of main changes
0.0	15.12.2016	Hmaied SHAIEK	Initial structure of the document
0.1	06.04.2017	Mouna BEN MABROUK	First contribution of Centrale Supélec included
0.2	28.04.2017	Hmaied SHAIEK and Daniel ROVIRAS	CNAM contribution included
0.2	01.05.2017	Daniel ROVIRAS	CNAM internal revision
0.2	05.05.2017	Mouna BEN MABROUK	Centrale Supélec internal revision
1.0	05.05.2017	Hmaied SHAIEK	First updation of the deliverable
1.1	11.05.2017	Hmaied SHAIEK	Second updation of the deliverable based on CEA review

Executive Summary

The main purpose of the WONG5 project is to study, analyze and compare the post-OFDM waveforms (WF)s in order to propose the most appropriate candidate for critical machine type communications. In Deliverable 2.1, an exhaustive study and comparison has been accomplished according to several criteria such as spectral efficiency, latency, asynchronous access related to both Timing offset and Carrier Frequency Offset, PAPR, Complexity and MIMO issues. Hence, a set of WFs that provide the best trade-off between these criteria has been defined. Taking advantage of Deliverable 2.1 output, in Deliverable 3.1 the performance of the selected WFs in terms of power spectral density (PSD), noise power ratio (NPR) and symbol error rate (SER) in the presence of a high power amplifier (HPA) is studied. Once the power amplifier presence is considered, it would be wise to study the different parameters influencing its operation mode. For this reason, a theoretical study about the PAPR complementary cumulative distribution function (CCDF) is hold in order to better understand the Delivrable 2.1 results about PAPR. Then, the PSDs of the considered WFs after power amplification is computed. Two power amplifier models are considered:

- A model considering the AM-AM modulations: Rapp model (theoretical model) [Rap91],
- A model considering the AM-AM and AM-PM modulations: polynomial model (realistic model proposed by the 3GPP) [RRy16].

Finally, the theoretical expression of the SER of the selected WFs in the presence of power amplifiers is detailed and confirmed by simulation results.

Table of Contents

1. Introduction

Multicarrier signals, due to Central Limit Theorem, have a high crest factor. Combined with non-linear High Power Amplifiers (HPA), this will create performances loss. All waveforms studied in D2.1 will be sensitive to HPA and non-linear amplification will result in two main drawbacks: The first one is Out of Band (OOB) radiation or spectral leakage/regrowth. This effect must be kept under a certain level characterized by transmission spectral masks. Because most of post OFDM waveforms have been proposed in order to have better frequency localization than classical CP-OFDM, the spectral effect of non-linear (NL) HPA has to be carefully studied and mitigated for these waveforms. The second drawback of a NL HPA is intermodulation products creating in-band non-linear noise and Bit Error Rate (BER) or Error Vector Magnitude (EVM) degradation.

The objectives of deliverable D3.1 are to study:

1. The crest factor of all waveforms that have been selected at the end of task 2.1 (selected waveforms of D2.1, part 5.1). A theoretical analysis of the Peak to Average Power Ratio (PAPR) of selected waveforms will be proposed together with simulation results,

2. The OOB radiation and the spectral regrowth due to NL HPA. Simulations of the spectral regrowth will be proposed for different values of the Input Back-Off (IBO) and two HPA models. One HPA is modelled by Rapp model and the other one is a polynomial model generated from measurements on a real HPA. Noise Power Ratio will be also investigated,

3. The Symbol Error Rate (SER) degradation due to NL HPA. Theoretical expressions of the SER will be proposed and compared with simulation results. As for OOB study, the two HPA models will be used.

In this deliverable, we present results about the degradations on spectrum and SER when NL HPA are used. At the light of performance degradations due to HPA it will be necessary to mitigate HPA effects. Non-linear effects mitigation will be studied and developed in deliverable D3.2.

This deliverable is organized as follows: section 2 recalls the different waveforms selected in D2.1 that will be studied and tested in D3.1 while section 3 gives insights on HPA characteristics and their effects. Section 4 studies theoretically the PAPR of the selected waveforms. Section 5 is devoted to HPA effects: OOB, Noise Power Ratio (NPR) and SER degradation. Finally section 6 concludes the deliverable.

2. Selected Waveforms

In deliverable D2.1 we have selected a set of candidate waveforms for C-MTC. All these selected waveforms will be taken into account in deliverable D3.1. As a reminder, the selected waveforms are:

Waveforms with complex orthogonality and windowing/filtering applied to a group of subcarriers:

- WOLA-OFDM
- UFMC/UF-OFDM
- f-OFDM

Waveforms with real orthogonality and filtering applied to single subcarrier:

- FBMC-OQAM

Waveforms without orthogonality and filtering applied to single subcarrier:

- FBMC-QAM

3. PA characteristics and effects

3.1 Introduction

In this chapter we will describe the main characteristics of the HPA in terms of amplitude and phase distortion. Some HPA models, commonly used in the literature, will be also described.

The NL HPA is commonly described by its input/output or transfer function characteristics. The amplitude to amplitude (AM/AM) and amplitude to phase (AM/PM) characteristics indicate the relationship between, respectively, the modulus and the phase variation of the output signal as function of the modulus of the input signal.

The system model to be considered in this report in given by figure 3-1.

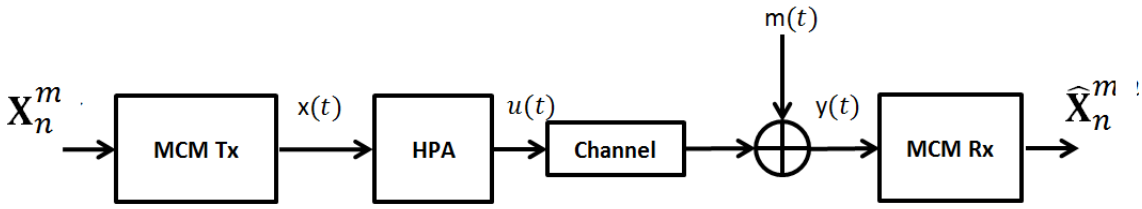

Figure 3-1: Basic sysem model.

The signal at the output of the Multi-Carrier Modulation (MCM) transmitter has a complex envelope $x(t)$. This signal can be written as

$$x(t) = \rho(t)e^{j\varphi(t)} \tag{3.1}$$

where

- $\rho(t)$ is the input signal modulus, and
- $\varphi(t)$ is the input signal phase.

If the HPA is linear, the signal at its output can be written as

$$u(t) = Gx(t) \tag{3.2}$$

where $G = |G|e^{j\phi_0}$ is a complex scalar which is constant with respect to $\rho(t)$.

In practice, the HPA cannot be considered as a linear device, i.e, $|G|$ and ϕ_0 constant with respect to $\rho(t)$. Then, as a general formulation, the amplified signal $u(t)$ can be written as

$$u(t) = F_a(\rho(t)) \exp(jF_p(\rho(t))) \exp(j\varphi(t)) \tag{3.3}$$

where

- $F_a(\rho(t))$ is the AM/AM characteristic of the HPA,
- $F_p(\rho(t))$ is the AM/PM characteristic of the HPA.

We can rewrite equation (3.3) as following

$$u(t) = S(\rho(t)) \exp(j\varphi(t)) \tag{3.4}$$

where $S(\rho(t)) = F_a(\rho(t)) \exp(jF_p(\rho(t)))$ is the complex soft envelope of the amplified signal $u(t)$.

The AM/AM and AM/PM characteristics cause distortions on the constellation scheme and spectral regrowth, degrading then the system performance. In practice, in order to avoid or at least to reduce the effects of nonlinearities, the HPA is operated at a given Input Back-Off (IBO) from its $1dB$ compression point [CGL09]. The $1dB$ compression point refers to the input power level where the transfer characteristics of the amplifier have dropped by $1\ dB$ from the ideal linear characteristics. An illustration of the $1dB$ compression point is given in figure 3-2.

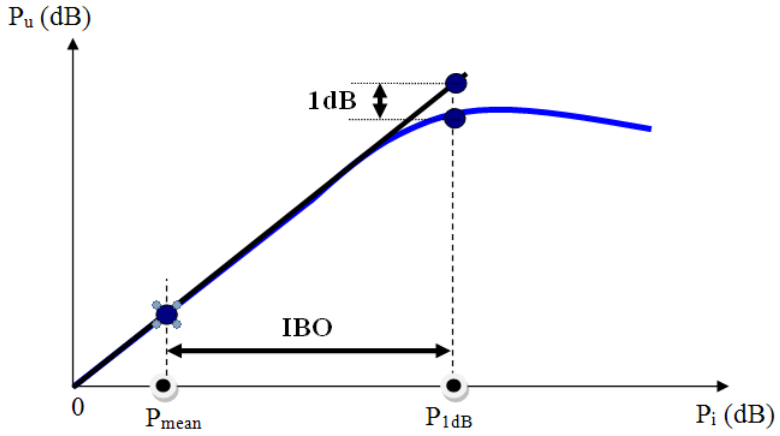

Figure 3-2: Typical AM/AM characteristic of a NL HPA.

In the log scale, the IBO is defined as follows:

$$\text{IBO} = 10 \log_{10} \left(\frac{P_{1\text{dB}}}{P_{mean}} \right) \tag{3.5}$$

where P_{1dB} is the input power at the $1dB$ compression point and P_{mean} is the mean input signal power.

For purpose of theoretical studies, it is necessary, for a given HPA, to propose a mathematical or physical model to reproduce or approximate its NL effects in amplitude (AM/AM) and phase (AM/PM). In the literature, two main families of HPA models can be found: the memoryless HPA models and the HPA models with memory. In this chapter, we will consider only memoryless HPA models.

The output of a memoryless HPA is a function of the input at a given time instant or after a fixed time delay. Any change in the input occurs instantaneously at the output. In frequency domain the zero-memory nonlinearity implies that the transfer characteristics are frequency independent.

Lets introduce, in the following section, some memoryless HPA models that will be used later in this report.

3.2 Memoryless HPA models

3.2.1 Soft Envelope Limiter

The Soft Envelope Limiter (SEL) is used for modeling a HPA with a perfect predistortion system. The global transfer function of the perfect predistortion followed by the HPA is thus a limiter which can be described by the following AM/AM and AM/PM functions:

$$\begin{aligned} F_a(\rho(t)) &= \begin{cases} \rho(t), \rho(t) \leq A_{\text{sat}} \\ A_{\text{sat}}, \rho(t) > A_{\text{sat}} \end{cases} \\ F_p(\rho(t)) &= 0 \end{aligned} \tag{3.6}$$

where A_{sat} is the HPA input saturation level.

3.2.2 Rapp model

This model, commonly used for modeling a Solid State Power Amplifiers (SSPA), was presented in [Rap91] and exhibits only AM/AM conversion. It can be expressed as

$$\begin{aligned} F_a(\rho(t)) &= \frac{\rho(t)}{(1+(\frac{\rho(t)}{A_{\text{sat}}})^{2p})^{\frac{1}{2p}}} \\ F_p(\rho(t)) &= 0 \end{aligned} \tag{3.7}$$

where p is a smoothness factor that controls the transition from the linear region to the saturation region, $(p > 0)$. This HPA model assumes a linear performance for low amplitudes of the input signal. Then, a transition towards a constant saturated output is observed. When $p \to \infty$, the Rapp model converges towards the SEL. In figure 3-3, we plot the AM/AM characteristics of the Rapp model for two values of the smoothness factor p.

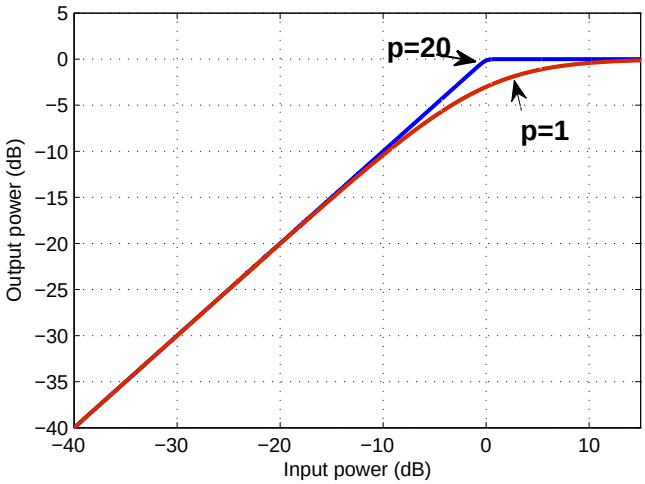

Figure 3-3: AM/AM characteristics of Rapp HPA model.

3.2.3 Saleh model

Saleh's model is generally used for modeling Travelling Wave Tube Amplifiers (TWTA) [Sal81]. This HPA model has been mainly used in several works dealing with the impact of nonlinearities in CP-OFDM systems [SM98, ZBR08]. According to this model, the AM/AM and AM/PM conversion characteristics can be expressed as follows:

$$F_a(\rho) = \frac{\alpha_a \rho(t)}{1 + \beta_a \rho(t)^2} \qquad (3.8)$$
$$F_p(\rho) = \frac{\alpha_p \rho(t)^2}{1 + \beta_p \rho(t)^2}$$

where α_a and β_a are the parameters to decide the NL amplitude distortion level, and α_p and β_p are phase displacements In figure 3-4, we plot the AM/AM and AM/PM characteristics of the Saleh model for different values of α_a, β_a, α_p and β_p.

In the literature we also found the following equations (3.9) for the modelling the AM/AM and AM/PM conversion characteristics of TWTA.

$$F_a(\rho) = A_{sat}^2 \frac{\rho(t)}{\rho(t)^2 + A_{sat}^2} \qquad (3.9)$$
$$F_p(\rho) = \varphi_0 \frac{\rho(t)^2}{\rho(t)^2 + A_{sat}^2}$$

where φ_0 controls the maximum phase distortion introduced by this HPA model. Its clear that both equations (3.8) and (3.9) allow the modeling of HPA exhibiting both NL amplitude and phase distortion.

3.2.4 Polynomial model

For purpose of theoretical analysis of NL HPA effects, it can be suitable to assume or approximate the transfer function of the HPA with a polynomial model. In this case the signal $u(t)$ at the output of the NL device can be written

$$u(t) = \sum_{l=1}^{L} a_l \rho(t) \left|\rho(t)\right|^{l-1} \qquad (3.10)$$

where

- L is the polynomial order, and
- a_l are the complex coefficients of the polynomial approximation.

In some works related to the study of spectral regrowth for CP-OFDM systems [ZK01], the polynomial models used, exhibit only odd coefficients for fitting the AM/AM and AM/PM curves. Note that in Zhou's work [ZR04], such HPA model is adopted because only odd order nonlinearities contribute to spectral broadening.

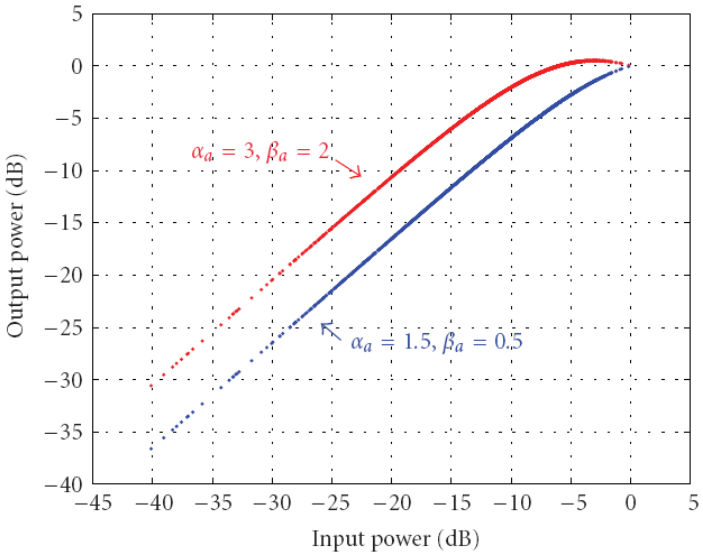

(a) AM/AM characteristics.

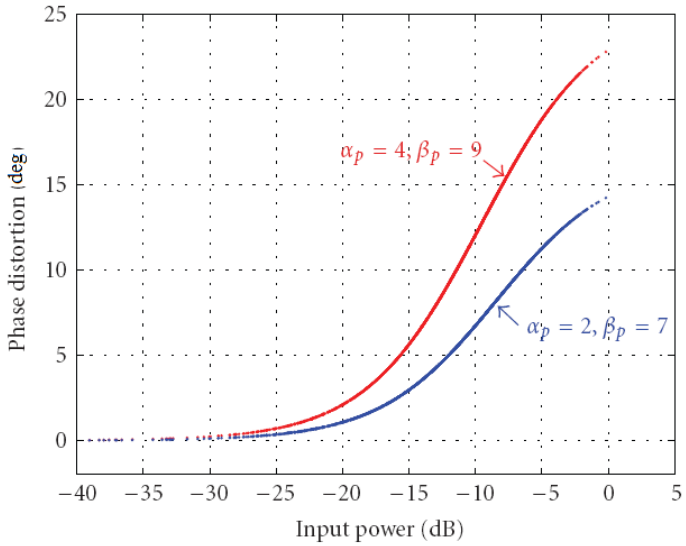

(b) AM/PM characteristics.

Figure 3-4: AM/AM and AM/PM characteristics of Saleh HPA model.

3.3 PAPR

Signals with high amplitude fluctuations, as in the case of MCM systems, pose a tough challenge to the RF design of a HPA. The power consumption helps defining the battery life for mobile communications systems [Lar98]. HPA represents more than 60% of the total power consumption at transmitter [BC11]. So, the PA linearity and energy efficiency are two vital parameters in the context of the signals with strong fluctuations, as evident in MCM techniques. In order to get rid of the amplified signal distortion, the HPA is made to operate in its linear region, which has very poor energy efficiency. The presence of high peaks cause IB and OOB interferences when the MCM signals are

passed through a HPA, which does not have enough linear range. The fluctuation of the signal envelope can be well understood by its PAPR. The PAPR is a random variable, which is a convenient parameter in measuring the sensitivity of a NL HPA, when a non-constant envelop input need to be transmitted. Low values of PAPR are synonymous with a transmitted signal with a power always very close to its mean power while high PAPR values indicate that the instantaneous power can be very high compared to the average one.

The PAPR of the continuous-time base-band signal $x(t)$ transmitted during a symbol period T is defined by,

$$PAPR_{x(t)} = \frac{\max_{0 \leq t \leq T} |x(t)|^2}{\frac{1}{T} \int_0^T |x(t)|^2 . dt} \tag{3.11}$$

3.4 HPA effects

HPA at the emitter side can be quasi linear for a certain part of the input powers, P_i, (from 0 to P_1, see Figure 3-5) and NL for input powers larger than P_1. Furthermore, the output power, P_u, is limited to a saturation power P_{sat} (Figure 3-5) for high values of P_i.

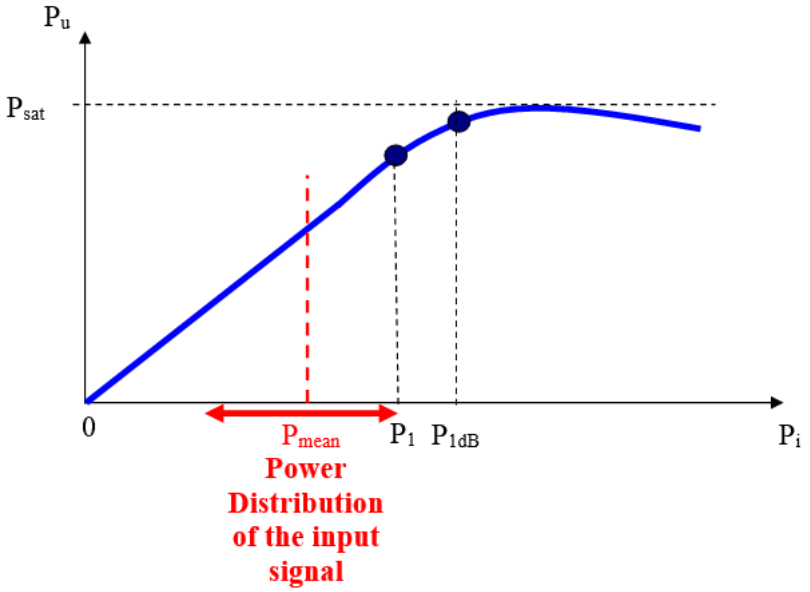

Figure 3-5: Linearized PA and input signal with low PAPR.

If the input power is always lower than P_1, the HPA is operated in its quasi linear region and the high PAPR of the MCM signal will not have any influence on the quality of the transmission. This is illustrated in Figure 3-5 by an input signal with a mean power equal to P_{mean} and a certain distribution of the input power around P_{mean}. Nevertheless, this situation has a high cost in terms of energy efficiency: operating a HPA with a very low mean input power gives a low mean output power compared to P_{sat}. Especially for C-MTC applications with batteries, it is necessary to increase the power efficiency. Real HPA communication systems will then be operated as close as possible to the saturation

point in order to increase the power efficiency. By doing that, two negative effects will appear:

- the output signal spectrum will be broadened compared to the input one,
- distortions will occur in the transmitted signal causing transmission errors.

These distortions result in effects in the band, which affect the quality of the signal and degrade the retrieval of information at the reception. As well as out-of-band effects that impact adjacent channels and cause interference between users.

3.4.1 In-Band effects

The quality of a transmission can be evaluated by calculating the BER or SER in order to be able to judge the degradations undergone by the transmitted signal. These degradations are function of the propagation channel characteristics, the transmission chain imperfections and the distortions caused by the non-linearities of the power amplifier. In Figure 3-6, we show, for illustration purpose, the performances of CP-OFDM in the presence of a Saleh HPA model with a nominal phase distortion $\varphi_0 = \pi/6$ and two IBO values equal to $4dB$ and $8dB$, for a Additive White Gaussian Noise channel (AWGN) and 16-QAM symbols.

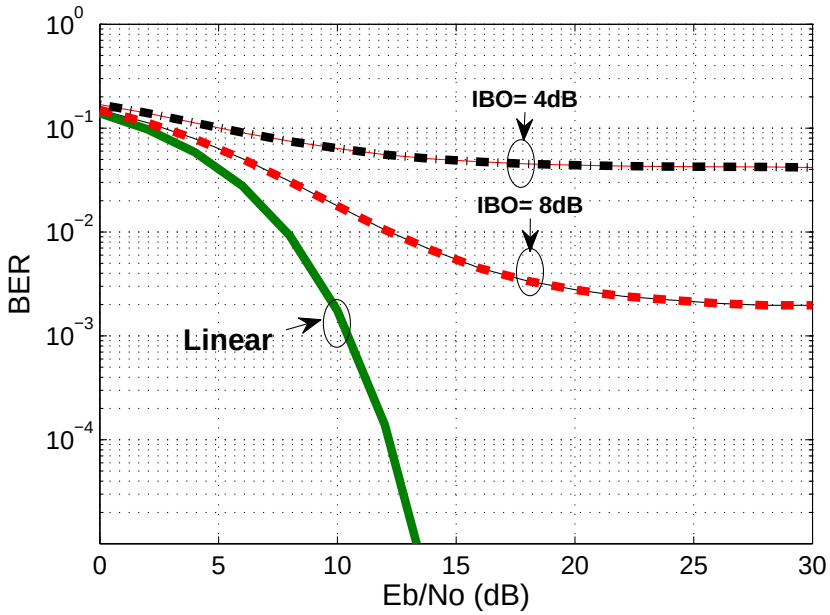

Figure 3-6: BER of CP-OFDM, $M = 64$, 16QAM, Saleh HPA, $\varphi_0 = \pi/6$, IBO=[6dB, 8dB], AWGN channel.

We recall that Eb/N_0 is the ratio of the Binary energy to the spectral density of the noise. According to figure 3-6, the degradations caused by the HPA on the BER of the CP-OFDM system is clearly established, as compared to the case of a perfect linear HPA. This degradation decreases when the IBO increases.

3.4.2 Out-Off-Band effects

The non-linear power amplifiers generate intermodulation products that will broaden the PSD of the signal at the output of the HPA.

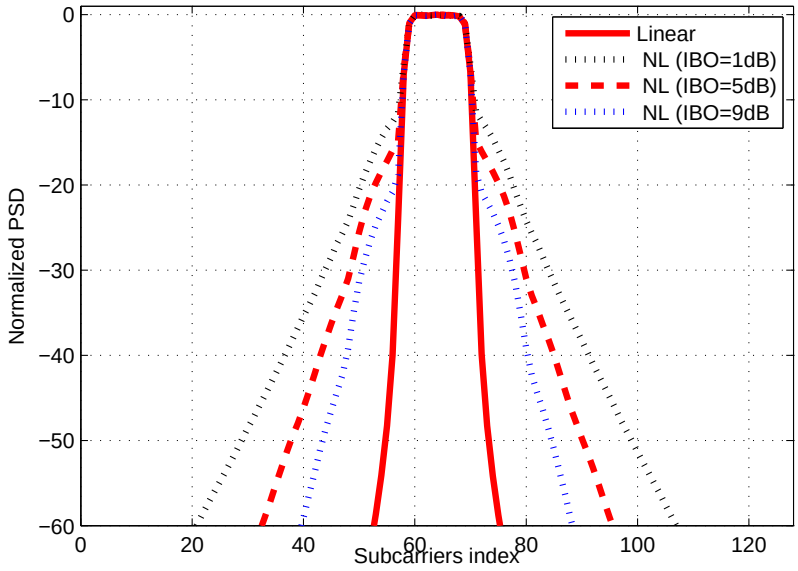

Figure 3-7: PSD of FBMC-OQAM system, 4QAM, Saleh HPA, $\varphi_0 = \pi/3$.

From the figure 3-7, we can observe the effect generated by the Saleh HPA model with $\varphi_0 = \pi/3$ on the spectrum of the FBMC-OQAM amplified signal as function of IBO. Indeed, the lower the is IBO, the higher is the spectral regrowth.

3.5 Mitigation of HPA effects

It's of prime importance with MCM systems to fight against NL amplification effects. Concerning distortions induced by the NL HPA, it is also important to limit and correct them. Looking at Figure 3-5, we can view several axes of progression concerning the NL effects of the HPA:

- we can increase the HPA linear area using PA linearization,
- we can decrease the distribution of high values of the instantaneous power of the transmitted signal. This is equivalent to lowering the PAPR of the transmitted MCM signal,
- we can also correct the NL distortion at the receiver side.

Increasing the HPA linearity together with PAPR minimization permits to increase power efficiency by increasing the mean power of the input signal, P_{mean}, very close to P_{sat}. If the HPA is perfectly linearized and if the PAPR is reduced to 0 dB (instantaneous power always very close to P_{mean}), the power efficiency can be very close to its maximum.. Furthermore, if the input signal is always in the linear region of the HPA, the

spectral regrowth will be limited. Thus, minimizing the impact of NL effects of HPA is mandatory and the most prevailing methods in literature, to deal with this are,

- Operate the PA with sufficient IBO,
- Reduce the PAPR of the modulated signal,
- Linearize the HPA characteristics.

4. PAPR analysis

In this part, a closed-form approximation of the PAPR for multi-carrier modulations is firstly proposed. Then, based on this approximation, a theoretical study is hold to define the necessary condition for waveforms with better PAPR than OFDM. Finally, the results of this analysis are discussed and their relevance is shown by simulation results.

4.1 PAPR optimization

In this section, we consider the generalized waveforms for multicarrier (GWMC) system. This system represents a large set of modulation schemes.

4.1.1 System model

The GWMC transmitted signal is expressed as

$$s_k = \sum_{n\in\mathbb{Z}} \sum_{m=0}^{M-1} x_{m,n} \underbrace{g_m[k-nP]}_{g_{m,n}[k]}, \tag{4.1}$$

where $x_{m,n}, n \in \mathbb{Z}, m \in [\![0, M-1]\!]$ are the transmitted symbols from a complex constellation, assumed to be independent and identically distributed with zero mean and variance σ_x^2, and $g_{m,n}[k]$ is the waveform filter, as depicted in Figure 4-1. P is the number of samples per waveform block.

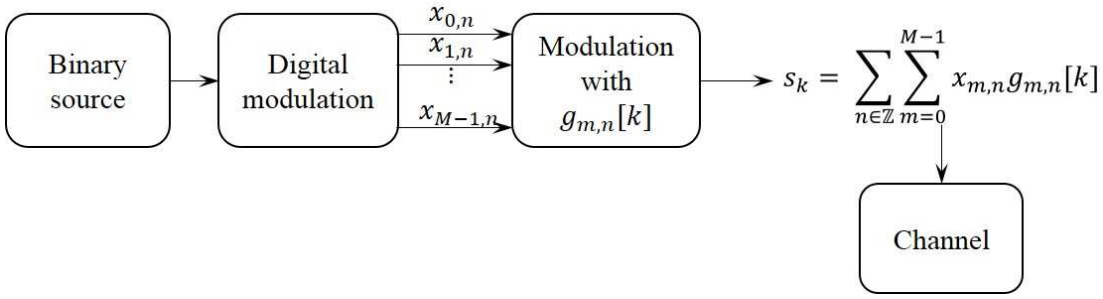

Figure 4-1: Multicarrier modulations general system model.

Based on Lyapunov central limit theorem, Chafii *et al.* proved in [CPG14] that the PAPR complementary cumulative distribution function (CCDF) of these multi-carrier modulations (MCM)s can be approximated as follows:

$$Pr(PAPR > \gamma) \approx 1 - \prod_{k\in[\![0,NM-1]\!]} (1 - e^{-c_k\gamma}), \tag{4.2}$$

where

$$c_k = \frac{\sum_{n\in\mathbb{Z}} \sum_{m=0}^{M-1} |g_{m,n}[k]|^2}{N \sum_{m=0}^{M-1} |g_{m,n}[k]|^2},$$

and N is the number of MCMs frames considered in the observation and γ is the PAPR threshold. This expression is reliable when the following conditions are satisfied:

- About the input symbols: the real and imaginary parts of $(x_{m,n})_{(m\in[\![0,M-1]\!],\, n\in\mathbb{Z})}$ are independent and identically distributed.

- About the waveforms: $\{g_m\}_{m\in[\![0,M-1]\!]}$ are bounded and have a finite temporal support:

$$A := \min_{m,k} \sum_{n\in\mathbb{Z}} |g_{m,n}[k]|^2 > 0. \tag{4.3}$$

  In other words, the temporal support of $g_{m,n}[k]$ has to be greater or equal to the symbol block period T i.e. containing M samples. This condition is denoted by First Condition in the remainder of this document.

- About the subcarrier number: The number of subcarriers is supposed to be $M \geq 8$. This is an assumption made for the validity of the central limit theorem [CPG14].

4.1.2 PAPR optimization problem

After establishing the PAPR CCDF expression, let us now build the PAPR optimization problem.

$$\begin{aligned} \underset{(g_m)_{m\in[\![0,M-1]\!]}}{\text{minimize}} \quad & Pr(PAPR > \gamma) \approx 1 - \prod_{k\in[\![0,NM-1]\!]} (1 - e^{-c_k\gamma}), \\ \text{subject to} \quad & A := \min_{m,k} \sum_{n\in Z} |g_{m,n}[k]|^2 > 0. \end{aligned} \tag{4.4}$$

Using the Riemann sum, it is straightforward to show that the PAPR optimization problem is equivalent to:

$$\begin{aligned} \underset{(g_m)_{m\in[\![0,M-1]\!]}}{\text{maximize}} \quad & \int_0^T \ln(1 - \mathrm{e}^{\frac{-\gamma \sum_{m=0}^{M-1} \|g_m\|^2}{T \sum_{n\in\mathbb{Z}} \sum_{m=0}^{M-1} |g_{m,n}(t)|^2}}) \, dt, \\ \text{subject to} \quad & A := \min_{m,k} \sum_{n\in Z} |g_{m,n}[k]|^2 > 0. \end{aligned}$$

4.1.3 Optimization problem solution

Let us now define as follows a critical value of γ, $\gamma_{\text{crit}}(\{g_m\})$, for a given GWMC:

$$\gamma_{\text{crit}}(\{g_m\}) := \sup_{t\in[0,T]} \frac{T \sum_{m=0}^{M-1} \sum_{n\in\mathbb{Z}} |g_{m,n}[k]|^2}{H_0 \sum_{m=0}^{M-1} \|g_m\|^2}. \tag{4.5}$$

γ is assumed to be greater than or equal to $\gamma_{\text{crit}}(\{g_m\})$ and $H_0 = 0.63$ [CPGB16]. For a system satisfying (4.3) and having γ greater than or equal to $\gamma_{\text{crit}}(\{g_m\})$ and

$$\sum_{m=0}^{M-1} \sum_{n\in\mathbb{Z}} |g^*_{m,n}[k]|^2 \quad \text{is constant over time.} \tag{4.6}$$

This condition is denoted by Second Condition in the remainder of this document.
For this system $\gamma_{\text{crit}}(\{g^*_m\}) = 1/H_0$ has the minimum possible value [CPG14] and $\{g^*_m\}$ denotes the optimal $\{g_m\}$. In other words, the GWMC system $\{g^*_m\}$ has optimal PAPR performance at level γ among all GWMC systems satisfying (4.3) and $\gamma \geq \gamma_{\text{crit}}(\{g_m\})$.

The condition in (4.6) means that the statistical mean of the instantaneous power of the transmitted signal $E(|x(t)|^2)$ is constant over time. This condition is verified for OFDM systems. In addition, as, for an OFDM system, $\gamma_{\text{crit}}(\{g^*_m\}) = 1/H_0$, the OFDM

is considered as an optimal solution for the optimization problem in subsection 4.1.2 [CPGB16].

We consider a GWMC system $\{g_m\}$ with $\gamma \geq \gamma_{\text{crit}}(\{g_m\})$. If this GWMC system has better PAPR performance at level γ than OFDM, then $\{g_m\}$ necessarily violates condition (4.3). Indeed, the fact that GWMC violates condition (4.3) means that the temporal support of at least one modulation function must be strictly smaller than the symbol period. Thus, we are led to a trade-off between frequency localization of multicarrier waveforms and PAPR performance.

4.2 Discussion

The condition $\gamma \geq \gamma_{\text{crit}}(\{g_m\})$ satisfied by a GWMC system means that our results are valid for the values of γ greater than a threshold value $\gamma_{\text{crit}}(\{g_m\})$.

For any GWMC system satisfying (4.3) such that OFDM system, we have $\gamma_{\text{crit}} \approx 2$dB. Our analysis does not cover the values of γ smaller than γ_{crit}. In practice, the PAPR of multicarrier modulation systems is greater than γ_{crit}. Thus, this interval does not represent an interval of interest.

All the assumptions and analysis made in Sections 4.1 and 4.2 can be applied to the considered waveforms by defining $g_{m,n}[k]$ for each one as follows:

- For UF-OFDM: The UF-OFDM signal is expressed as:

$$\begin{aligned} s_k &= \sum_{n\in\mathbb{Z}} \sum_{b=0}^{B} \sum_{p=(b-1)N_B}^{bN_B-1} x_{p,n} e^{j2\pi\frac{np}{M}} f^b[k-nM]. \\ s_k &= \sum_{n\in\mathbb{Z}} \sum_{m=0}^{M} x_{m,n} e^{j2\pi\frac{mn}{M}} f^{\lfloor\frac{n}{N_B}\rfloor}[k-nM]. \end{aligned} \tag{4.7}$$

  So that

$$g_{m,n}^{UF-OFDM}[k] = e^{j\frac{2\pi mn}{M}} f^{\lfloor\frac{n}{N_B}\rfloor}[k-nM]. \tag{4.8}$$

  where $\lfloor\cdot\rfloor$ is the floor function, B is the number of the allocated resource blocks, N_B is the number of subcarrier per resource block and $f^{\lfloor\frac{n}{N_B}\rfloor}$ is the filter per resource block.

- For F-OFDM: As the F-OFDM signal can be written as follows:

$$s_k = \sum_{n\in\mathbb{Z}} \sum_{m=0}^{M-1} x_{m,n} f[k-nM] e^{j2\pi\frac{mk}{M}}, \tag{4.9}$$

  where M_g is the cyclic prefix length and f is the spectrum shaping filter, we have:

$$g_{m,n}^{F-OFDM}[k] = f[k-nM] e^{j2\pi\frac{mk}{M}} \tag{4.10}$$

- For WOLA-OFDM: A WOLA-OFDM signal can be written as follows:

$$s_k = \sum_{n\in\mathbb{Z}} \sum_{m=0}^{M-1} x_{m,n} p[k-nM] e^{j2\pi\frac{m(k-nM)}{M}}, \tag{4.11}$$

  Therefore,

$$g_{m,n}^{WOLA-OFDM}[k] = p[k-nM] e^{j2\pi\frac{m(k-nM)}{M}}. \tag{4.12}$$

- For FBMC-OQAM: The FBMC-OQAM function is defined as:

$$g_{m,n}^{FBMC-OQAM}[k] = h_{OQAM}(k - nM)e^{(j2\pi\frac{m}{M}(k-D/2))}e^{j\theta_{m,n}},$$

then $|g_m(k-nN)|^2 = h_{OQAM}^2(k-nN)$, where h_{OQAM} is the prototype filter, D is the prototype filter overlapping factor and $\theta_{m,n} = \frac{\pi}{2}(m+n) - \pi mn$.

- For FBMC-QAM: The FBMC-QAM signal can be written as below:

$$s_k = \sum_{n\in\mathbb{Z}}\sum_{m=0}^{M-1} x_{m,n}p[k - nM]e^{j2\pi\frac{m(k-nM)}{M}}, \tag{4.13}$$

Therefore,

$$g_{m,n}^{FBMC-QAM}[k] = p[k - nM]e^{j2\pi\frac{m(k-nM)}{M}}. \tag{4.14}$$

The filters: $g_{m,n}^{UF-OFDM}$, $g_{m,n}^{F-OFDM}$, $g_{m,n}^{WOLA-OFDM}$, $g_{m,n}^{FBMC-OQAM}$ and $g_{m,n}^{FBMC-QAM}$ are designed to have a better frequency localization than the rectangular filter used in OFDM. These filters have variable amplitude during the symbol time T. Consequently, they do not verify the first condition. For this reason, they have a different PAPR CCDF curve compared to the OFDM one. In addition, the temporal support of these filters is greater or equal to the symbol time T. Therefore, they verify the First condition. For this reason, the PAPR of these waveforms is greater than the OFDM level.

Figure 4-2 summarizes the conclusions of this study.

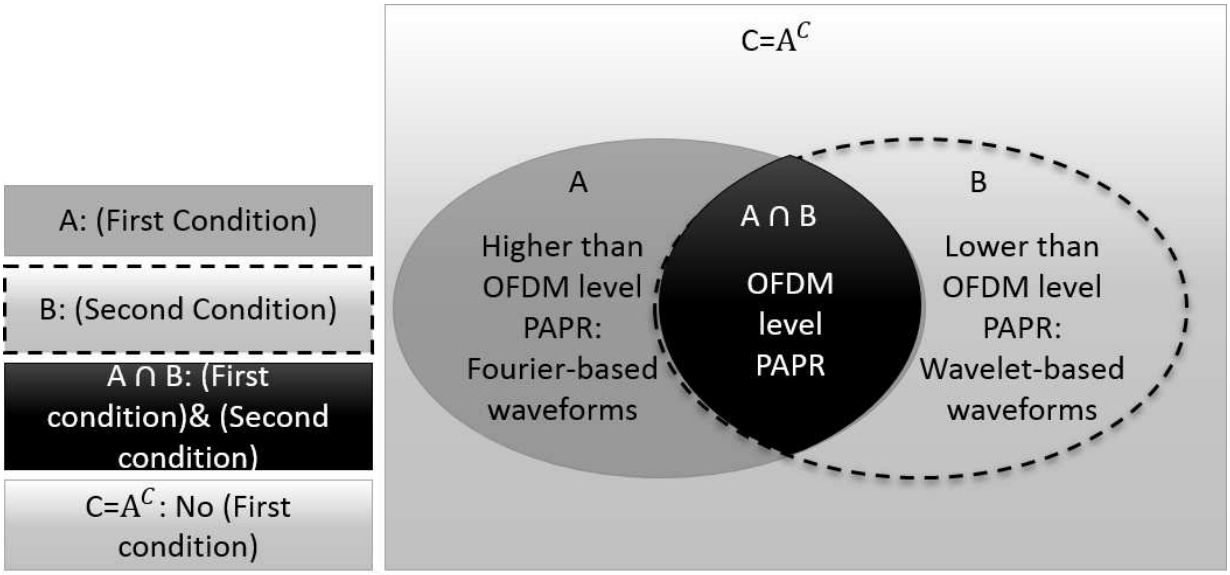

Figure 4-2: Classification of the waveforms regarding the PAPR performance.

We can observe from Figure 4-3, for a given number of subcarriers, that traditional CP-OFDM provides the best PAPR performance, which is in line with our analysis. Note that the block size N_{Block} used for the PAPR computation is the same for all the waveforms and has been set to 1024 since it refers to the size of the traditional CP-OFDM block symbol as configured for LTE (10MHz).

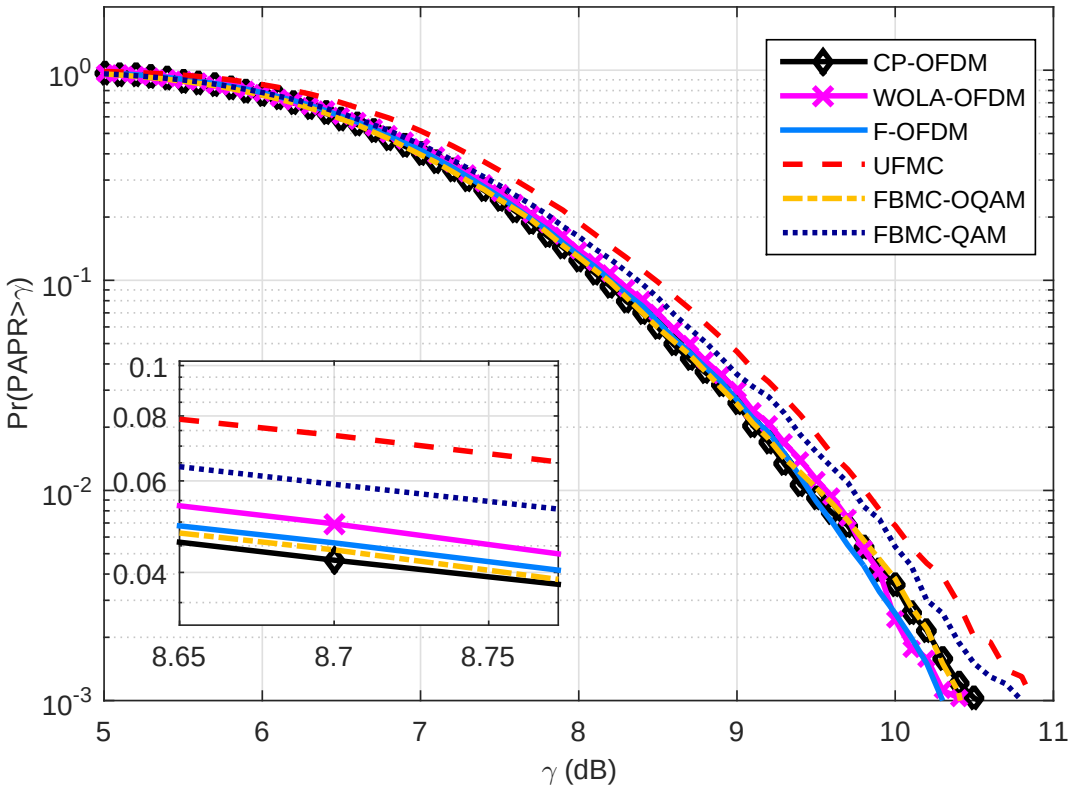

Figure 4-3: PAPR CCDF- based comparison between the selected waveforms.

5. Analysis and simulation of PA effects

5.1 System model

In this study, we consider a scenario of two coexisting users sharing the available frequency band as depicted in Figure 5-1, where the dashed area and the red colored one correspond to the time/frequency resources allocated to the user of interest and the other one, respectively. The useful signal occupies a frequency band of 540 kHz equivalent to 3 LTE resource blocks (LTE-RB bandwidth = 180 kHz) while 1.62 MHz (i.e. 9 LTE-RB) are allocated to the other user on each side of the useful frequency band.

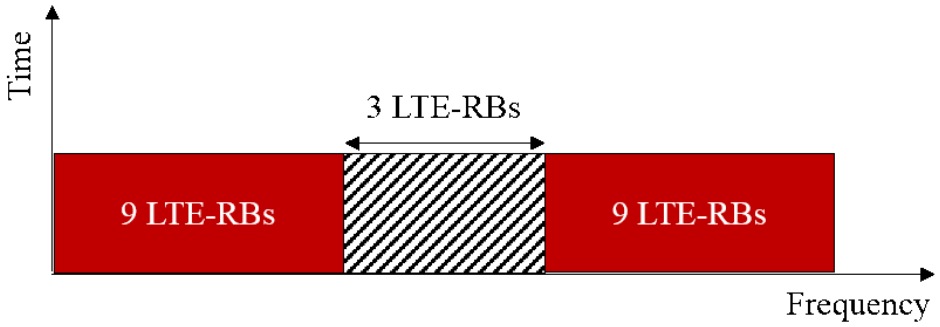

Figure 5-1: Coexistence scenario.

Our purpose in this Section is to identify the amount of the generated-noise power in the dashed area. For this reason, the output signal of each waveform spectrally localized on the red colored area is amplified using two PA models. More details about these models will be given in Section 5.1.2. Hence, a PSD-based comparison is firstly hold between the considered waveforms in this task for different IBOs. Then, the noise power ratio (NPR) variation with the IBO in the dashed area is presented and analyzed. It should be noted that there is no signal transmitted in the dashed area to be able of properly evaluating the noise power.

Finally, in order to highlight the impact of the PA on the considered waveforms spectral localization and bit-error-rate (BER), we consider AWGN channels between both transmitters on one side and the receiver of interest on the other side. So that, all the considered users have a perfect time/frequency synchronization.

5.1.1 Parameters

In this section, we provide the general parameters of the scenario previously described (see Table 5-1) as well as specific parameters related to the different waveforms considered in this document:

- Waveforms with complex orthogonality: Tables 5-2,
- Waveforms with real orthogonality: Table 5-3,
- Non-orthogonal: Table 5-4.

Table 5-1: General parameters

General	
RB bandwidth	180 kHz
Useful bandwidth of user of interest (UOI)	540 kHz
Input data	16-QAM
Subcarrier spacing	15 kHz
Sampling Frequency	15.36 MHz

Table 5-2: Waveforms with complex orthogonality

CP-OFDM / WOLA-OFDM	
FFT size	1024
CP length	72
Windowing	Raised cosine
Window length (W_e,W_r)	$(20, 32)$
UFMC (UF-OFDM)	
FFT size	1024
Filter	Dolph-Chebyshev
Filter length ($\mathrm{L_{FIR}}$ =ZP+1)	73
Zero padding length	72
Stop-band attenuation	40 dB
Receive windowing	Raised cosine
f-OFDM	
FFT size	1024
Filter	the same at both Tx and Rx sides
Filter length	512
CP length	72
Transition band	2.5 $\times$ 15 kHz
Burst truncation	CP/2 on each side

Table 5-3: Waveforms with real orthogonality

FBMC-OQAM	
Prototype Filter	PHYDYAS
Overlapping factor (K)	4
FFT size	1024

Table 5-4: Non orthogonal waveforms

FBMC-QAM	
Prototype Filter	Samsung Type I [YKK$^+$15]
Overlapping factor (K)	4
FFT size	1024

5.1.2 Chosen HPA models: characteristics and parameters

As the used signal in the WONG5 context is a narrow-band signal, the memory effects of the HPA are not significant. For this reason, for this task, we use two memoryless models. The first one, the Rapp model, considers only the AM/AM conversion. The second model, a polynomial model provided by [R4-16], considers both AM/AM and AM/PM conversions. In the remainder of this Section, the characteristics of the chosen models are detailed.

5.1.2.1 Polynomial model

The complex envelop of a MCM signal (see figure 3-1) can be expressed as:

$$x(t) = \rho(t)\exp(j\varphi(t)), \tag{5.1}$$

where $\rho(t)$ and $\varphi(t)$ are respectively the signal modulus and phase.

The model used in this Section is a 4 GHz HPA realistic polynomial model provided by [R4-16]. It represents a HPA with both AM/AM and AM/PM conversions. In this case, the HPA output signal can be written as follows:

$$u(t) = F_a(\rho(t))\exp(jF_p(\rho(t)))\exp(j\varphi(t)), \tag{5.2}$$

where $F_a(\cdot)$ and $F_p(\cdot)$ are respectively the AM/AM and AM/PM conversion functions. They are expressed as follows:

$$F_a(\rho(t))\exp(jF_p(\rho(t))) = \sum_{n=1}^{L} a_n \rho(t)^n. \tag{5.3}$$

where a_n, $n = 1 \cdots L$ are the polynomial model coefficients of the complex soft envelope $F_a(\rho(t))\exp(jF_p(\rho(t)))$ of the amplified signal and L the polynomial model order. This model is denoted for the remainder of this document by 3GPP HPA. It is based on a measured HPA. Indeed, the AM/AM and AM/PM data are measured from a commercial 4 GHz long term evolution (LTE) user equipment HPA. The measured AM/AM and AM/PM curves were approximated using $L = 9$.

Hence, the two polynomials given in [R4-16] model correspond to an AM/AM conversion from dBm to dBm and an AM/PM conversion from dBm to degrees.

To obtain the AM/AM and AM/PM conversions caused by the HPA on the input signal when the latter is in volts, we follow the upcoming steps:

1. The first step is to plot AM/AM curve from $P_{indBm} = -35dBm$ to $+10dBm$. We obtain the AM/AM curve depicted in Figure 5-2:

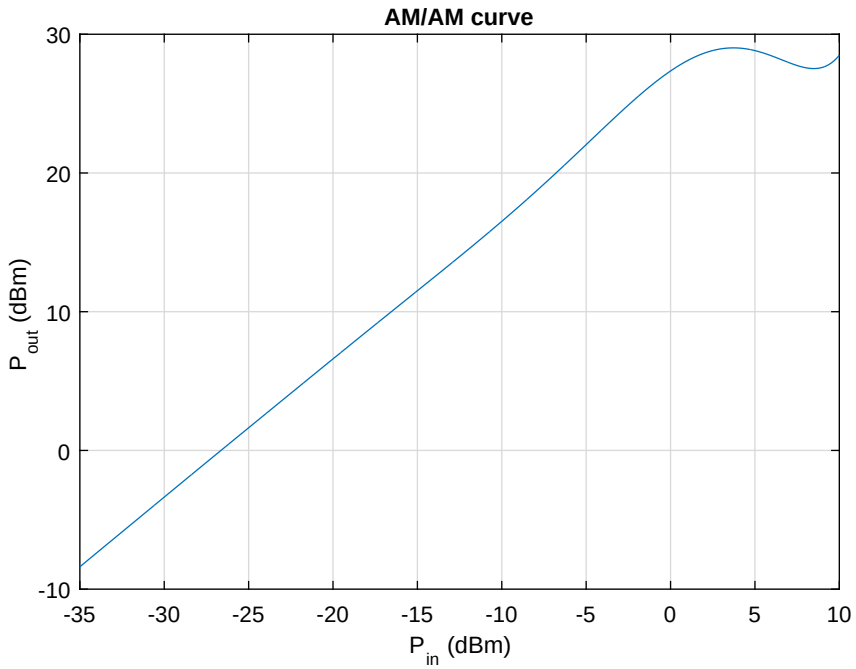

Figure 5-2: 3GPP HPA model: AM/AM conversion, input in dBm, output in dBm.

2. The second step is to retrieve the AM/AM curve from $P_{indBm} = -35dBm$ to $+10dBm$, using this time volts instead of dBm for x axis. The conversion from dBm to voltages is given by:

$$P_{inLin} = 1e-3 * 10.^{(P_{indBm}/10)}, \quad (5.4)$$

$$V_{inLin} = \sqrt{(P_{inLin} * R)} \quad (5.5)$$

where $R = 50\ \Omega$ is the HPA input impedance.
The range [-35dBm +10dBm] corresponds to [0.004V 0.7V]. Outside this voltage range, the polynomial expression is no more valid.

3. On Figure 5-3, we can see that the AM/AM curve from v=0 to v=0.2 is different from a straight line. It is necessary to have a constant gain for low voltages. From v=0 to v=0.2 we will replace the original AM/AM curve (blue) by a straight line (red). A new AM/AM conversion curve is then obtained.

4. Using the new AM/M conversion, the polynomial coefficients are estimated.

5. For AM/PM conversion, we do the same: (a) AM/PM conversion from dBM to radian (See Figure 5-4) , (b) AM/PM conversion from volts to degrees, (c) estimation of the polynomial coefficients. Finally, we obtain the AM/PM curve in Figure 5-5.

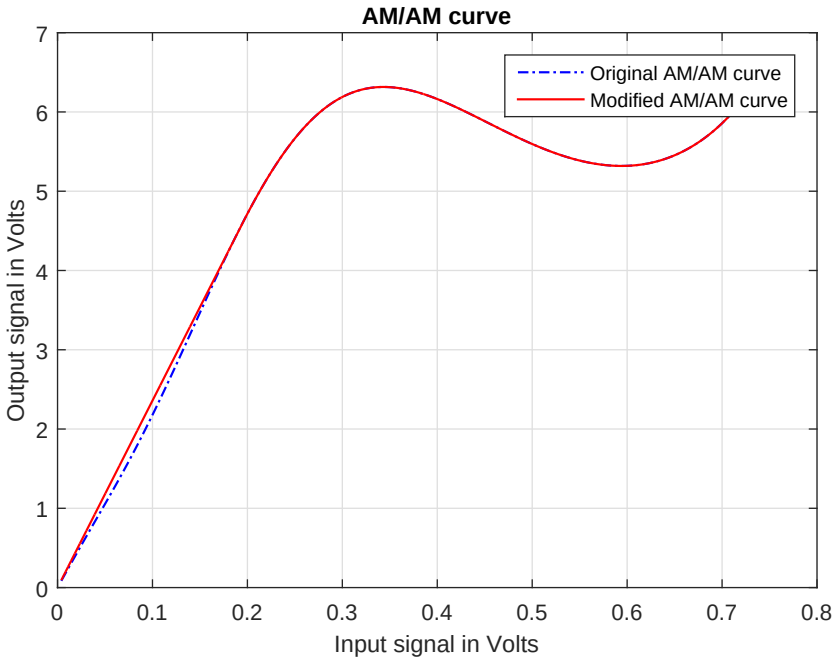

Figure 5-3: 3GPP HPA model: AM/AM conversion, input in volts, output in volts.

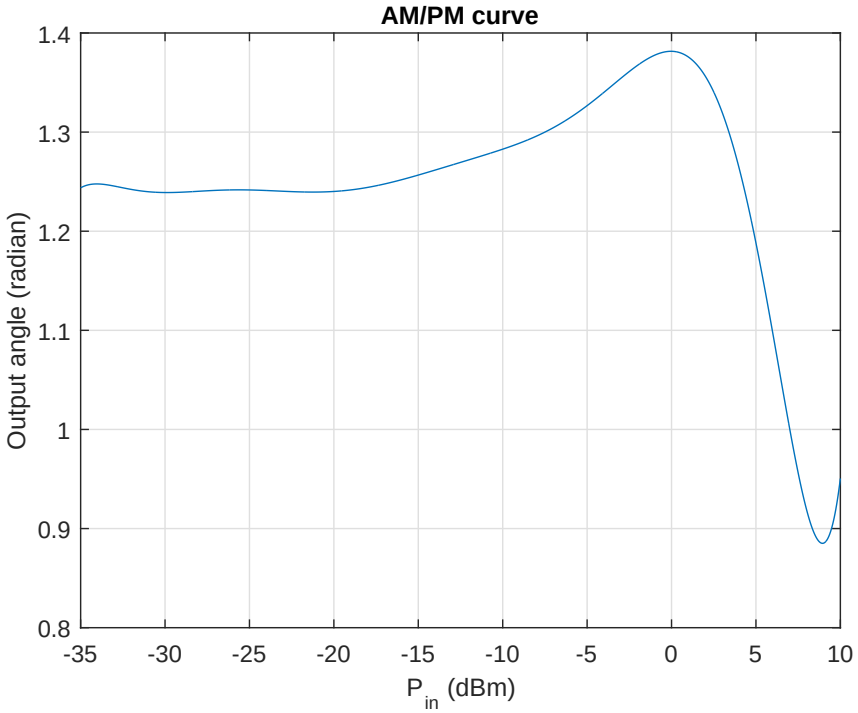

Figure 5-4: 3GPP HPA model: AM/PM conversion, input in dBm, output in radian.

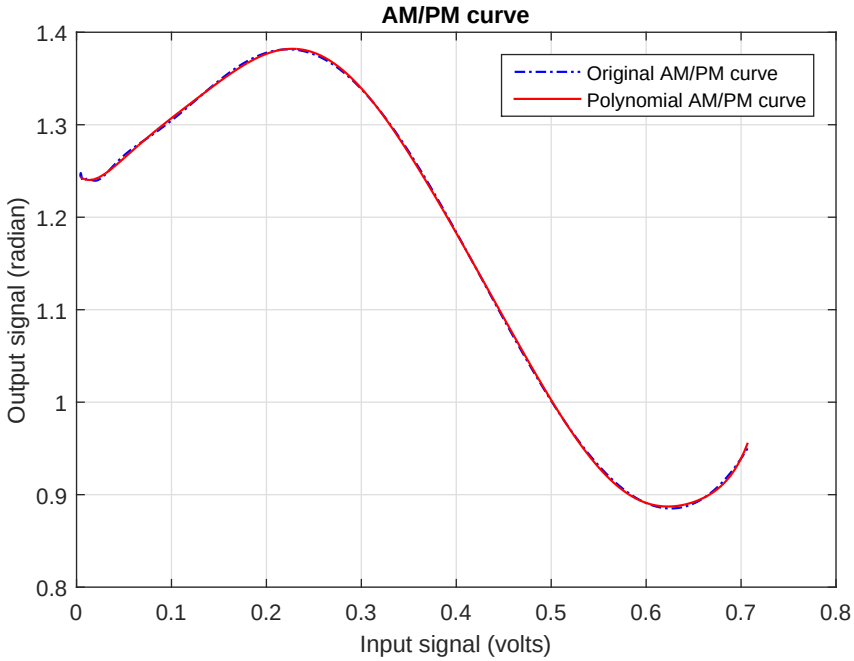

Figure 5-5: 3GPP HPA model: AM/PM conversion, input in volts, output in radian.

5.1.2.2 Rapp model

The signal at the HPA output can be written as follows:

$$u(t) = F_a(\rho(t))\exp(j\varphi(t)), \tag{5.6}$$

where $\rho(t)$ and $\varphi(t)$ are respectively the input signal modulus and phase. $F_a(\cdot)$ is the AM/AM conversion function, expressed as follows:

$$F_a(\rho(t)) = \frac{G\rho(t)}{\left(1+\left|\frac{G\rho(t)}{A_{sat}}\right|^{2p}\right)^{\frac{1}{2p}}} \tag{5.7}$$

where G is the linear gain and A_{sat} is the saturation voltage. It should be noted that G and A_{sat} are chosen to be the same as the polynomial model previously detailed. p is chosen to be 1.1 to have a different -1dB compression point from the 3GPP HPA as it can be seen in Figure 5-6.

5.2 PSD

Using the waveform parameters defined in Table 5-1, 5-2, 5-3 and 5-4, and the HPA models defined in Section 5.1.2, we hold a comparison between the considered waveforms in terms of frequency localization and BER after amplification. Indeed,in this Section, the impact of non-linear power amplification with and without phase distortion on the waveforms PSD, NPR and BER is studied. For the BER, analytical results will be proposed in addition to the simulation ones.

We present in Figures 5-7, 5-8, 5-9, 5-10, 5-11 and 5-12 the PSD comparison of the considered waveforms. It has been well established in Deliverable 2.1 that the CP-OFDM has poor frequency domain localization compared to the other waveforms considered in WONG5 project. However, after non-linear power amplification, in-band and

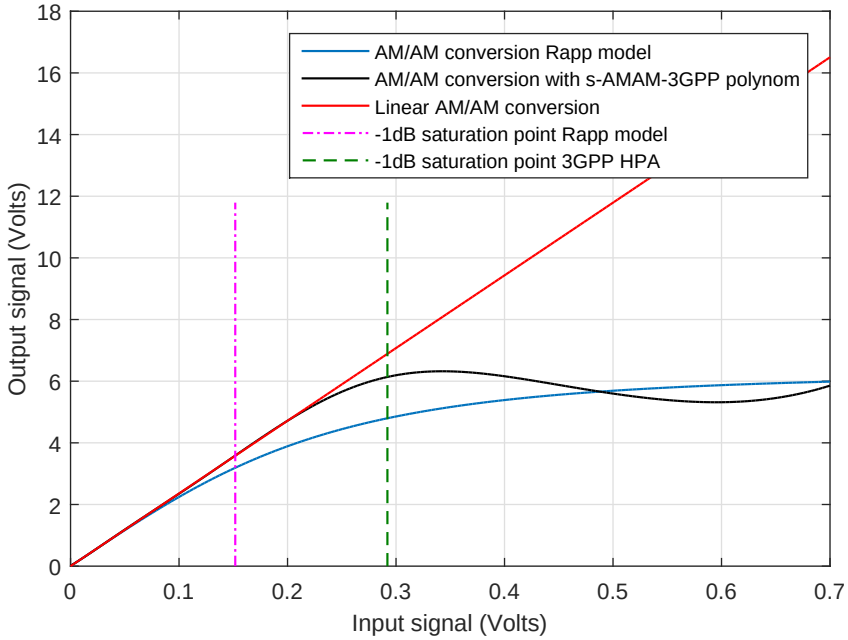

Figure 5-6: Rapp model: AM/AM-conversion comparison between the Rapp model and the 3GPP HPA, input in volts, output in radian.

out-of-band radiations are introduced. Consequently, the PSD tails become higher. In this section, we study the frequency domain localization resistance to this phenomenon. In other words, the PSD of the considered waveforms after power amplification is compared to the CP-OFDM amplified one in order to verify if their PSD advantage is kept even after HPA. Indeed, good or excellent spectral containment will be a key parameter for future 5G waveform in order to support neighboring and non orthogonal signals especially after power amplification.

- For $IBO = 0dB$, the HPA operates in its compression region where the amplification is non-linear. For this reason, the PSD tails of the considered waveforms become higher. However, the impact of the non-linear power amplification is not the same on the PSD tail level for each waveform. Indeed, when the power amplifier cause AM/PM distortion the CP-OFDM provide the worst PSD level. On the other side, one can notice from Figure 5-7 that the difference between the considered WFs PSD levels is not significant. This is not the case when the HPA model does not consider the AM/PM distortions. Here, the PSD of the CP-OFDM is significantly the worst. Also, from Figure 5-8, a slight difference between the remaining WFs can be noticed. In this case, FBMC-QAM, FBMC-OQAM and Filtered-OFDM show the lowest PSD tails level. It should be noted that the PSD tails levels are lower when using the Rapp model than the case of the 3GPP HPA.

- For $IBO = 5dB$: At this operation point, the HPAs are less non-linear than the previous case. Hence, their impact on the WFs spectral shapes is less significant than the previous case. Nevertheless, the 3GPP HPA still generating higher OOB than the Rapp case. When using the latter, the considered WFs frequency-localization are distinguishable. Indeed, in Figure 5-10, the WOLA-OFDM shows the highest PSD tails. As expected, the lowest PSD tails are given by FBMC-QAM, FBMC-

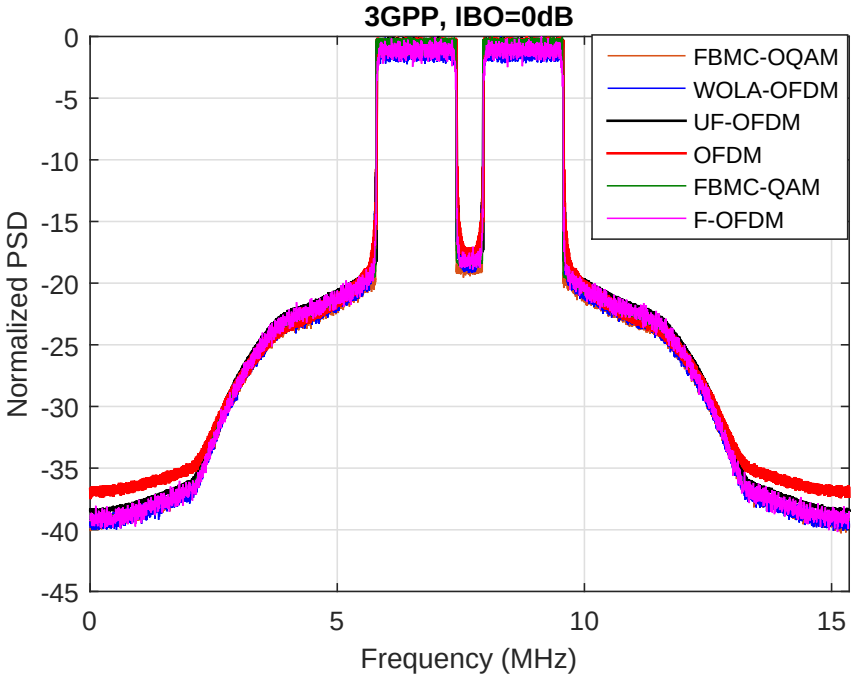

Figure 5-7: PSD-based comparison between FBMC-QAM, FBMC-OQAM , UF-OFDM, F-OFDM, CP-OFDM and WOLA-OFDM at the 3GPP HPA model output for IBO=0dB.

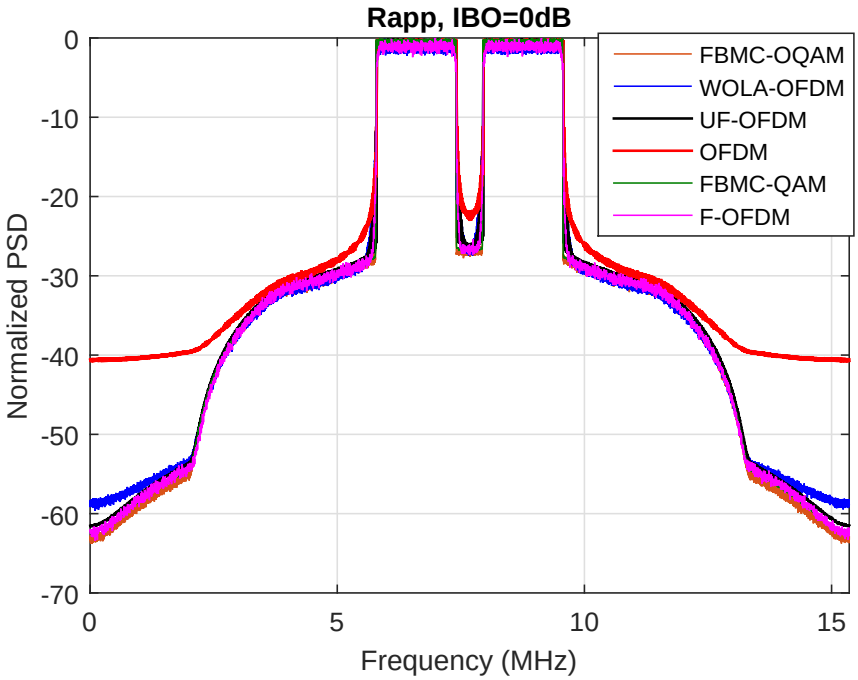

Figure 5-8: PSD-based comparison between FBMC-QAM, FBMC-OQAM , UF-OFDM, F-OFDM, CP-OFDM and WOLA-OFDM at the Rapp model output for IBO=0dB.

OQAM and Filtered-OFDM. Indeed, their PSD tails are from the beginning very low compared to CP-OFDM and WOLA-OFDM. Therefore, as the amplification is becoming linear, the OOB emissions of each waveform is getting back its level. On the other hand, there is no significant difference between the WFs OOB emissions at the output of the 3GPP HPA.

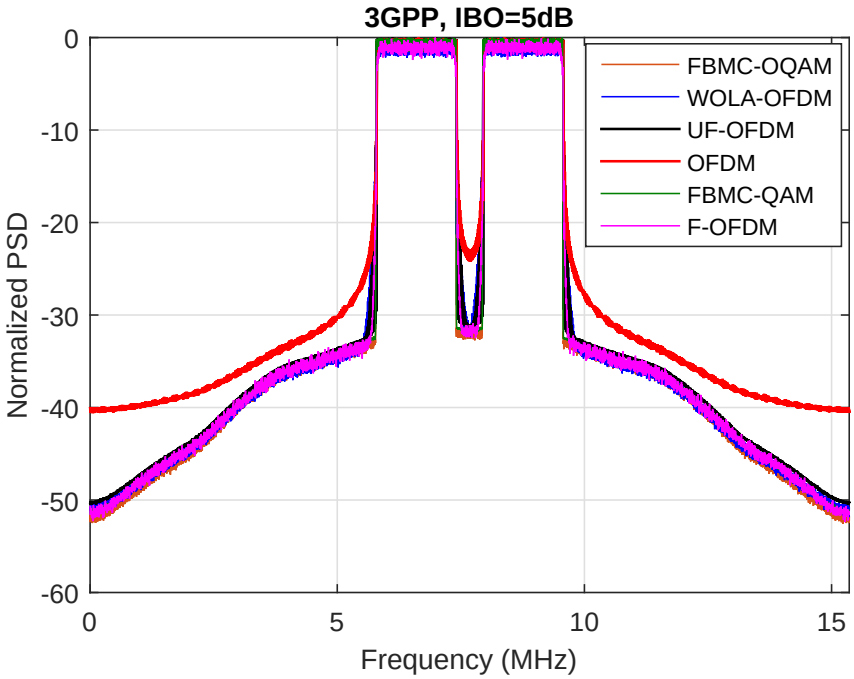

Figure 5-9: PSD-based comparison between FBMC-QAM, FBMC-OQAM , UF-OFDM, F-OFDM, CP-OFDM and WOLA-OFDM at the 3GPP HPA model output for IBO=5dB.

- For $IBO = 12dB$: This operating point is significantly far away from the compression region. For this reason, the Rapp model is considered linear at this operating point. See Figure 5-12. However, this is not the case of 3GPP HPA model as it still has AM/PM distortions. These distortions as it has been said previously make the OOB emissions at the output of the 3GPP more significant than the Rapp case. From Figure 5-11, one can notice this phenomenon as no significant difference between the PSD-tails of the considered WFs is distinguished.

To summarize, at the output of a HPA generating AM/PM distortions and at an IBO=0 dB, the considered WFs have no advantage in terms of frequency localization compared to CP-OFDM. However, at higher IBOs the FBMC-QAM, FBMC-OQAM , UF-OFDM and F-OFDM have better PSD performance than WOLA-OFDM and CP-OFDM. This improvement is no more significant using HPAs with AM/PM distortions.

This analysis is hold to check the performance of the considered WFs in terms of OOB emissions in terms of PSD shape. Let us now evaluate it using the noise power level generated in the dashed area (Figure 5-1) variation with in the IBO.

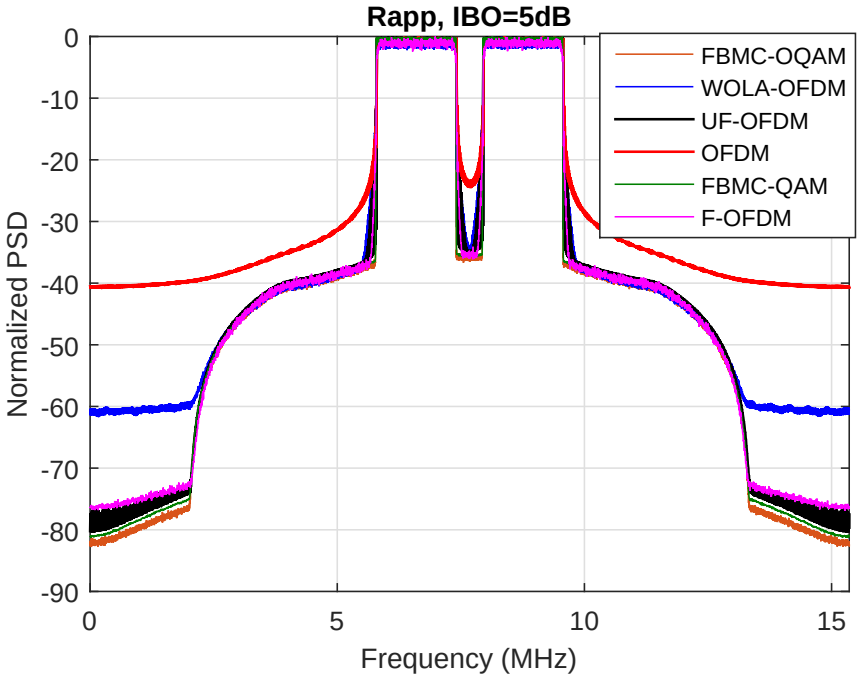

Figure 5-10: PSD-based comparison between FBMC-QAM, FBMC-OQAM , UF-OFDM, F-OFDM, CP-OFDM and WOLA-OFDM at the Rapp model output for IBO=5dB.

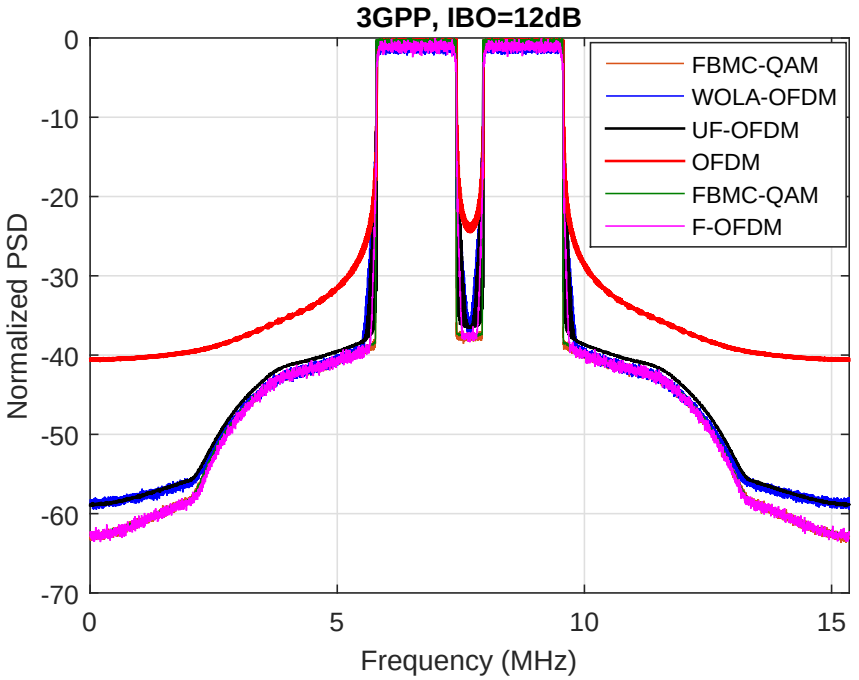

Figure 5-11: PSD-based comparison between FBMC-QAM, FBMC-OQAM , UF-OFDM, F-OFDM, CP-OFDM and WOLA-OFDM at the 3GPP HPA model output for IBO=12dB.

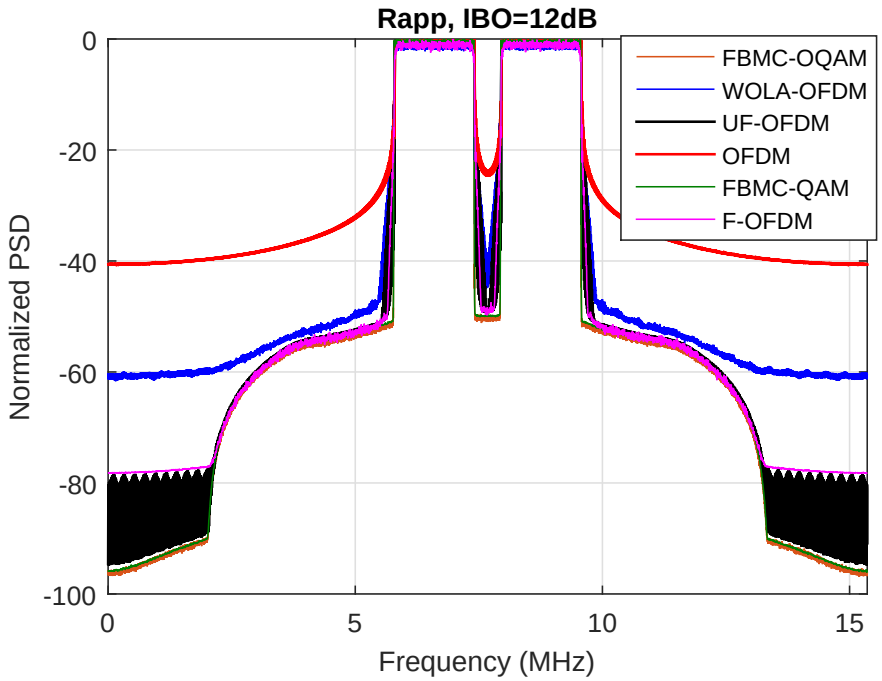

Figure 5-12: PSD-based comparison between FBMC-QAM, FBMC-OQAM , UF-OFDM, F-OFDM, CP-OFDM and WOLA-OFDM at the Rapp model output for IBO=12dB.

5.3 NPR

5.3.1 With 3GPP HPA model

Two zones can be distinguished:

- IBO $\leq$ 4 dB: For all the considered WFs, the NPR decreases with a slope of almost 2.5 when the IBO increases. In this region, the behavior of the HPAs is changing significantly from the non-linear to the linear behavior.
- IBO $\geq$ 4 dB: For all the considered WFs, the NPR decreases with a smaller slope when the IBO increases. In this case, the HPA behavior is already linear regarding the AM/AM distortions but still causing the AM/PM distortions. This makes the NPR stagnates for the CP-OFDM and WOLA-OFDM. However, for FBMC-QAM, FBMC-OQAM , UF-OFDM and F-OFDM, their filtering systems protect them from these distortions.

The WFs can be classified according to the NPR level from the best to the worst as: 1.FBMC-QAM, 2.FBMC-OQAM , 3.UF-OFDM, 4.F-OFDM, 5.CP-OFDM, 6.WOLA-OFDM. For FBMC-QAM and FBMC-OQAM a slight difference is noticed when the IBO is under 6 dB. They show the same performance when the IBO is greater than 6 dB.

5.3.2 With Rapp model

As it has been said previously, that with the Rapp model we have distortions with lower severeness. For this reason, the NPR levels for all the WFs is lower than the case of the 3GPP HPA. The decreasing slope of the NPR in this case is no more significant unless for the case of FBMC-QAM and FBMC-OQAM. In the case of the latter, the NPR

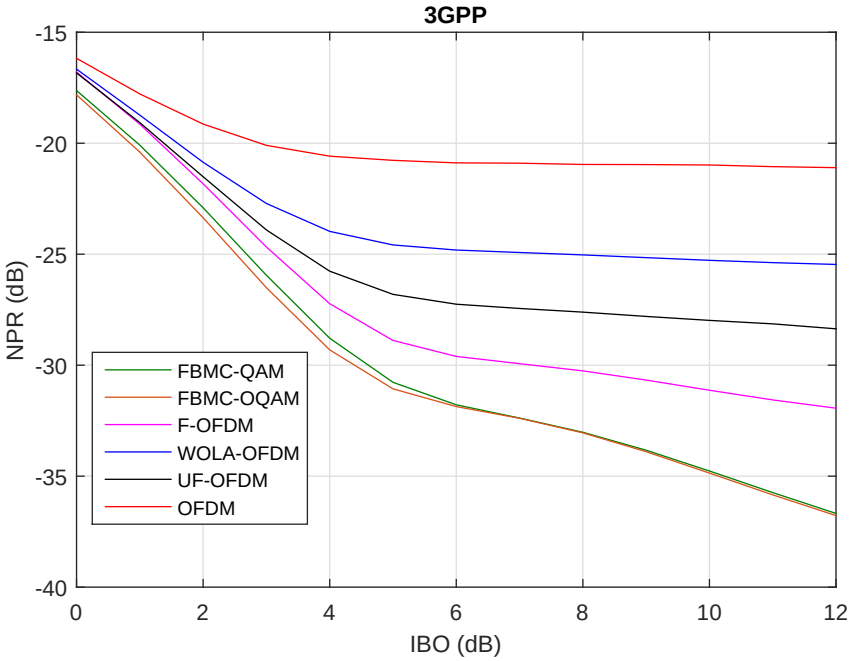

Figure 5-13: NPR-based comparison between FBMC-QAM, FBMC-OQAM , UF-OFDM, F-OFDM, CP-OFDM and WOLA-OFDM at the 3GPP HPA model output.

is approximately a linear function of the IBO with a slope of 1.5. The WF classification done for the 3GPP HPA still valid for the Rapp model.

5.4 SER

5.4.1 Considered Waveforms

We have used two HPA models for the simulations. The first one (HPA1) is a polynomial HPA model from [RRy16]. With this HPA1 model we have AM/AM distortion together with AM/PM distortion. The second HPA model is a Rapp modified model. The linear gain of the Rapp model has been taken equal to the linear gain of HPA1. With HPA2 model we have only AM/AM distortion. Six Waveforms have been tested for the two HPAs with different IBOs and different parametrizations.

- **WF1**: classical CP-OFDM with $Mfft = 1024$ subcarriers.
- **WF2**: WOLA-OFDM with CP being the CP length and Wt being the length of the transmission window. The transmission window is the Meyer RRC window. WOLA-OFDM has 1024 subcarriers.
- **WF3**: UFMC with a filter with length equal to $Lg = 73$ and a sideband attenuation of $40dB$. The number of used subcarriers is the maximum one, equal to $\lfloor Mfft/12 \rfloor /12$.
- **WF4**: f-OFDM. The number of used subcarriers is equal to $Mfft \times 31/32 = 992$ subcarriers. The transmission and reception filter has a length equal to 512. An f-OFDM frame is composed of Framelength OFDM classical symbols with CP. The

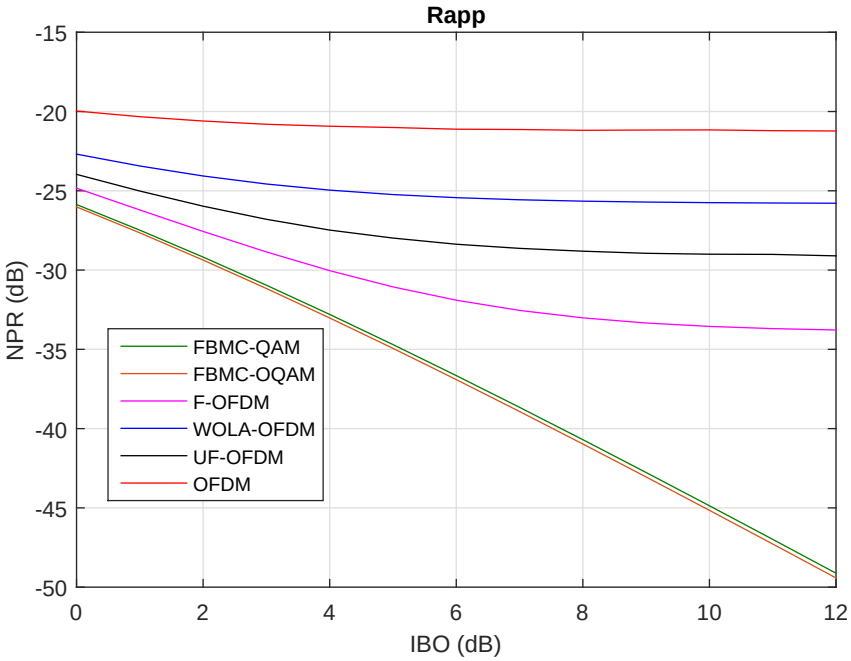

Figure 5-14: NPR-based comparison between FBMC-QAM, FBMC-OQAM , UF-OFDM, F-OFDM, CP-OFDM and WOLA-OFDM at the Rapp model output.

time domain signal is then filtered by the transmission filter and truncation is applied both at the beginning and at the end of the time domain signal. Truncation duration is equal to $CP/2$ as shown in figure 5-15.

- **WF5**: FBMC-OQAM with $Mfft = 1024$ subcarriers and the PHYDYAS filter with overlapping $K = 4$.
- **WF6**: FBMC-QAM with $Mfft = 1024$ subcarriers and the SAMSUNG-II filter[1].

5.4.2 Theoretical computation of SER performance

For computing the analytical performance in terms of SER/BER of the different WFs, we have used the Bussgang theorem and followed the same analysis as in [BSR+14]. When the input HPA signal $x(t)$ can be considered as a Gaussian signal, the Bussgang theorem states that the output HPA signal $u(t)$ can be expressed as:

$$u(t) = Kx(t) + d(t) \tag{5.8}$$

where K is a complex gain and $d(t)$ a complex zero mean noise uncorrelated with $x(t)$. K and σ_d^2 can be computed, based on expressions given in [DTV00], by:

$$K = \frac{1}{2}E\left[\frac{\partial S(\rho)}{\partial \rho} + \frac{S(\rho)}{\rho}\right] \tag{5.9}$$

where E is the expectation operator. We recall that $S(\rho) = F_a(\rho)\exp(jF_p(\rho))$ is the complex soft envelope of the amplified signal $u(t)$. The variance σ_d^2 of the NL distortion

[1]Remark: for FBMC-QAM, the theoretical expression of the SER is very difficult to obtain because of the iterative behavior of the receiver. In this deliverable, no SER results will be given for FBMC-QAM.

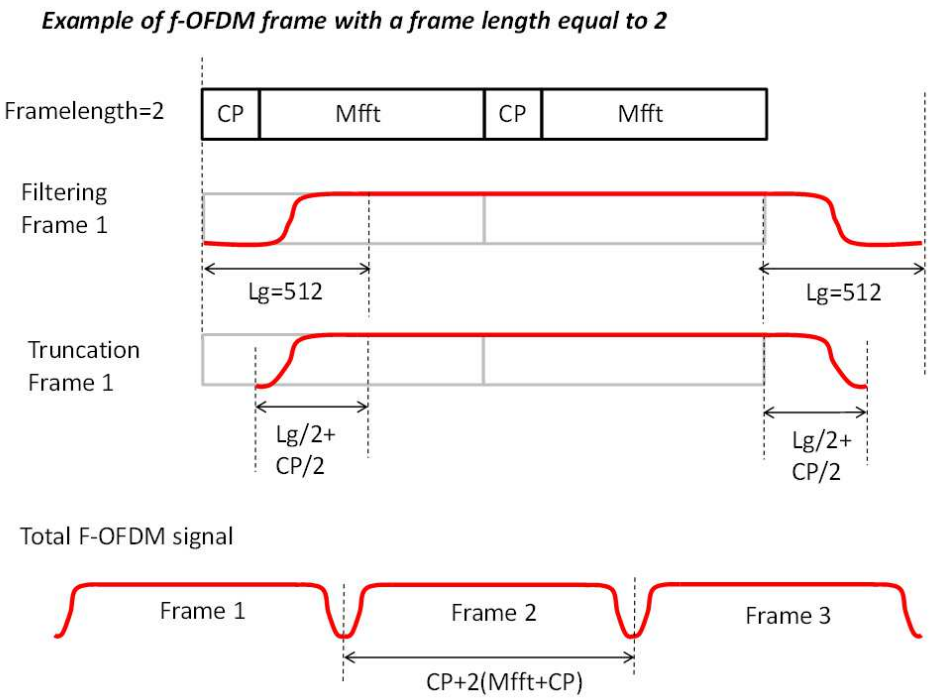

Figure 5-15: f-OFDM frame.

$d(t)$ is given by the following equation

$$\sigma_d^2 = E(|d(t)|^2) = E\left(|S(\rho)|^2\right) - |K|^2 E(\rho^2) \tag{5.10}$$

In order to compute analytically K and σ_d^2 we have followed the proposed method of [BSR+14], consisting in identifying the polynomial behavior of the HPA as:

$$u(t) = \sum_{n=1}^{L} a_n x(t) |x(t)|^{n-1} \tag{5.11}$$

where

- L is the polynomial order,
- a_n are the complex coefficients of the polynomial approximation.

Using the polynomial approximation of $S(\rho)$ we have :

$$S(\rho) = \sum_{n=1}^{L} a_n \rho^n \tag{5.12}$$

K and σ_d^2 can be computed using

$$K = \frac{1}{2} \sum_{n=1}^{L} (n+1) a_n E\left[\rho^{n-1}\right] \tag{5.13}$$

The variance σ_d^2 of the NLD $d(t)$ given in (5.10) becomes

$$\sigma_d^2 = \sum_{n=1}^{L} |a_n|^2 E\left[\rho^{2n}\right] + 2 \sum_{n,l=1,n\neq l}^{L} \Re[a_n a_l^*] E\left[\rho^{n+l}\right] - |K|^2 E\left[\rho^2\right] \tag{5.14}$$

where $\Re[.]$ stands for the real part.

The above theoretical expressions of K and σ_d^2 involve the computation of the expectation of ρ^n (n is a positive integer). This expectation is equivalent to calculate the n^{th} derivation of the Moment-Generating Function (MGF).

We can write $E[\rho^n]$ as

$$E[\rho^n] = \left.\frac{\partial^n M(t)}{\partial t^n}\right|_{t=0} \tag{5.15}$$

where

- n is a positive integer,
- $M(t)$ is the MGF given by

$$M(t) = E[e^{\rho t}] \tag{5.16}$$

A generic expression for the computation of $E[\rho^n]$ is given in [RQZ04]. It is expressed as follows

- For odd values of n we have

$$\begin{aligned} E\left[\rho^n\right] &= \left.\frac{\partial^n M(t)}{\partial t^n}\right|_{t=0} \\ &= \sqrt{\frac{\pi}{2}}\sigma^n \prod_{i=0}^{\frac{n-1}{2}}(2i+1) \end{aligned} \tag{5.17}$$

- For even values of n we have

$$\begin{aligned} E\left[\rho^n\right] &= \left.\frac{\partial^n M(t)}{\partial t^n}\right|_{t=0} \\ &= (\sqrt{2}\sigma)^n(\frac{n}{2})! \end{aligned} \tag{5.18}$$

where ! stands for the factorial operator.

Using equations (5.13), (5.17) and (5.18), we have finally for the NL parameter K

$$\begin{aligned} K = a_1 &+ \sqrt{\frac{\pi}{8}} \sum_{n=2,\ n\ even}^{L} (n+1)a_n\sigma^{n-1} \prod_{i=0}^{\frac{n-2}{2}}(2i+1) \\ &+ \frac{1}{2} \sum_{n=3,\ n\ odd}^{L} (n+1)a_n(\sqrt{2}\sigma)^{n-1}(\frac{n-1}{2})! \end{aligned} \tag{5.19}$$

For the variance σ_d^2 of the NL noise $d(t)$, we obtain the following expression

$$\begin{aligned} \sigma_d^2 = &\sum_{n=1}^{L} |a_n|^2 2^n\sigma^{2n}n! - 2|K|^2\sigma^2 \\ &+ \sqrt{\frac{4\pi}{2}} \sum_{n,l=1,n\neq l,\ (n+l)\ odd}^{L} \Re[a_n a_l^*]\sigma^{n+l} \prod_{i=0}^{\frac{n+l-1}{2}}(2i+1) \\ &+ 2 \sum_{n,l=1,n\neq l,\ (n+l)\ even}^{L} \Re[a_n a_l^*](\sqrt{2}\sigma)^{n+l}(\frac{n+l}{2})! \end{aligned} \tag{5.20}$$

Having a non linear HPA, the use of Bussgang theorem, is similar to an extra noise given by $d(t)$ and with variance σ_d^2. The SER theoretical performance is then given by:

$$SER_{theo}(E_b/N_0) = 2(1 - \frac{1}{\sqrt{M}})erfc(\sqrt{\frac{|coeff_{IBO_{m1dB}}|^2 3log2(M)}{2(M-1)N_{0theo}}}) \quad (5.21)$$

with:

- $N_{0theo} = log2(M).(\sigma_d^2 + \sigma_w^2)/|K|^2$ is the total noise power corresponding to both non-linear noise $d(t)$ and thermal noise $w(t)$.
- $\sigma_w^2 = var(u(t))/(log2(M).E_b/N_0)$ is the thermal noise corresponding to E_b/N_0.
- $coeff_{IBO_{m1dB}}$ is the coefficient applied on the input signal in order to have the right IBO at the HPA input,
- M is the size of QAM constellation.

5.4.3 Comparison between theoretical and simulated SER performance

Concerning OFDM and FBMC-OQAM, we have similar performances for different IBOs and HPAs. Concerning WOLA, UFMC and f-OFDM, the performance is lower than the one of OFDM because of the gap between different frames.

5.4.3.1 WOLA case

For WOLA we have a signal with a constant mean power on each sample except at the beginning and at the end of the WOLA-OFDM symbol. Each $CP + Mfft + Wtx$ samples we have a diminution of the samples power due to the windowing application. The windowing process is presented on figure 5-16.

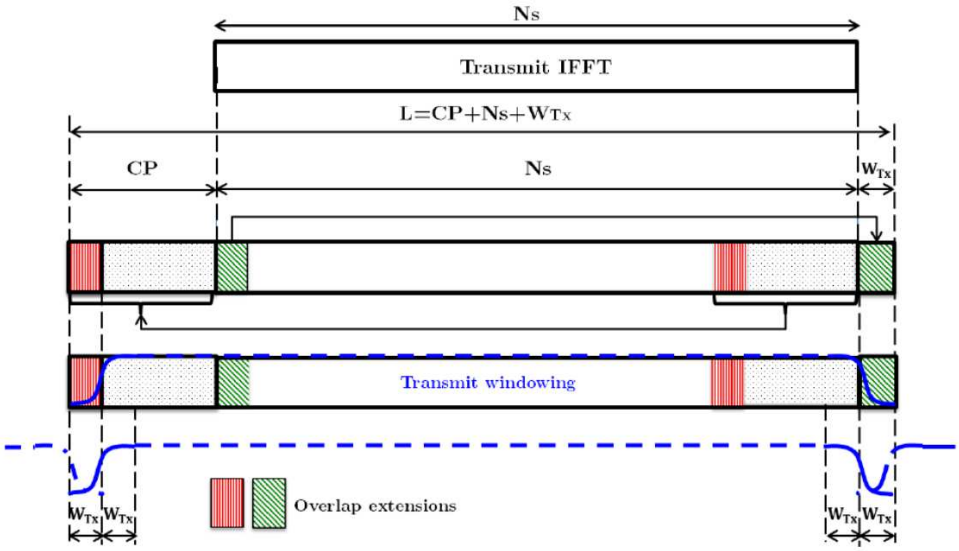

Figure 5-16: WOLA-OFDM transmitted signal.

Finally we have the WOLA signal represented in figure 5-17.

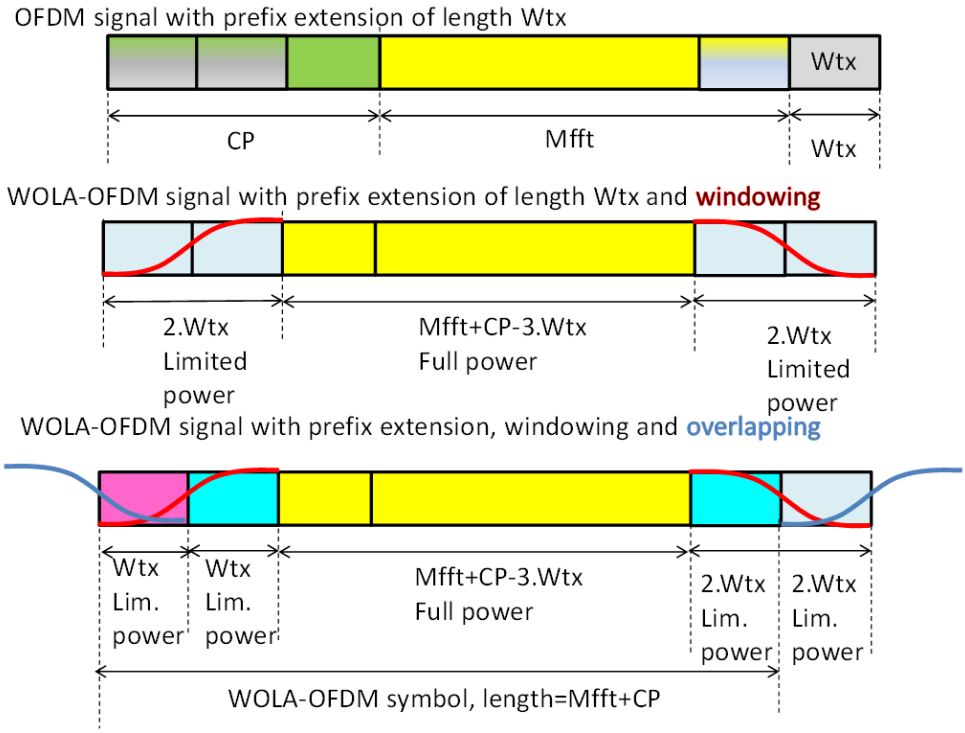

Figure 5-17: WOLA-OFDM signal power.

The mean power of one single WOLA-OFDM (of length $Mfft+CP$) symbol is equal to:

$$P_0(Mfft+CP+3.Wtx)+2P_0\sum_{k=1}^{Wtx}Wtx(k)^2+2P_0\sum_{k=W_tx}^{2Wtx}Wtx(k)^2 \quad (5.22)$$

where P_0 is the mean power per OFDM sample.

The mean power of a WOLA-OFDM symbol is lower than the one of OFDM. Then, for reaching the same IBO, the WOLA-OFDM signal has to be amplified in order to have an equivalent IBO as OFDM. For the crests of the WOLA-OFDM signal, this is equivalent as having an equivalent lower IBO. Figure 5-18 presents the time domain mean power per sample of a WOLA-OFDM signal with Mfft=1024, CP=72 and Wtx=30. We clearly see on figure 5-18. that, every $(Mfft+CP+Wtx)$ samples there is a diminution of the mean power due to the windowing effect. The width of the "'hole"' between the areas where the mean power is constant is equal to $3Wtx$ samples.

The gain that has to be applied to the WOLA-OFDM time domain signal is equal to:

$$\Delta_G=\frac{P_0(Mfft+CP)}{P_0(Mfft+CP+3.Wtx)+2P_0\sum_{k=1}^{Wtx}Wtx(k)^2+2P_0\sum_{k=Wtx}^{2Wtx}Wtx(k)^2} \quad (5.23)$$

This extra gain corresponds to an equivalent IBO for WOLA-OFDM equal to:

$$IBO_{WOLA-OFDM}=IBO_{OFDM}-10log10(\Delta_G) \quad (5.24)$$

The theoretical SER for WOLA-OFDM has the same expression as the SER of OFDM except that coefficients K and σ_d^2 are computed for the equivalent $IBO_{WOLA-OFDM}$ given by equation (5.24).

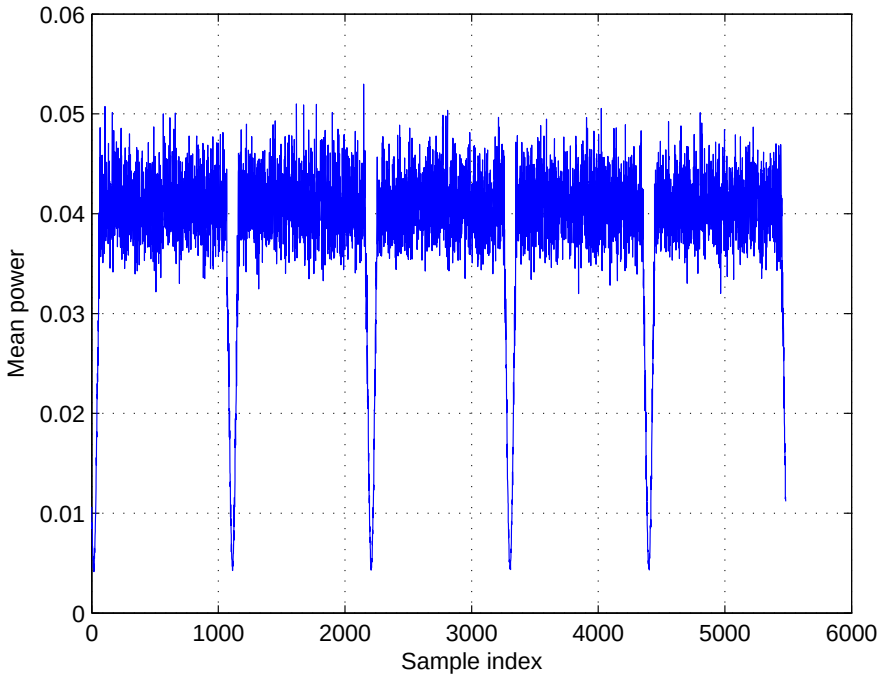

Figure 5-18: WOLA-OFDM mean power per sample.

Figure 5-19 presents the SER of WOLA-OFDM for $Mfft = 1024$, $CP = 72$, $Wtx = Wrx = 20$, 64-QAM and for HPA2 with three IBOs= 2, 3 and $4dB$. There is a very good match between theoretical expressions and simulation results.

Figure 5-20 presents the SER of WOLA-OFDM for $Mfft = 1024$, $CP = 256$, 64-QAM, HPA2 with $IBO = 4dB$ and various values of Wtx. When Wtx is increasing, the length of the holes in figure 5-18 is increasing, yielding a higher IBO and thus a lower SER performance. We can see on figure 5-20 that there is a good match between theoretical expressions and simulation results

5.4.3.2 UFMC case

As for WOLA, we have a signal with a constant mean power on each sample except at the beginning and at the end of the UFMC symbol. Each $CP + Mfft$ samples we have a diminution of the samples power due to the filtering at the transmitter side. The filtering process is presented on figure 5-21.

In figure 5-21, we see that there are three regions in a UFMC symbol:

- from time domain sample $k = 0 : Lg - 1$ (blue part of UFMC symbol, figure 5-21)
- from time domain sample $k = Lg : Lg + Mfft - 1$ (yellow part of UFMC symbol)
- from time domain sample $k = Lg + Mfft : Lg + Mfft + Lg - 1$ (green part of UFMC symbol)

where Lg is the impulse response filter length. If we call $[s(0), s(1), \ldots, s(Mfft-1)]$ the $Mfft$ OFDM time domain samples, after filtering we have $[c(0), c(1), c(2), \ldots, c(Mfft-1+Lg)]$ non zero samples. and we have

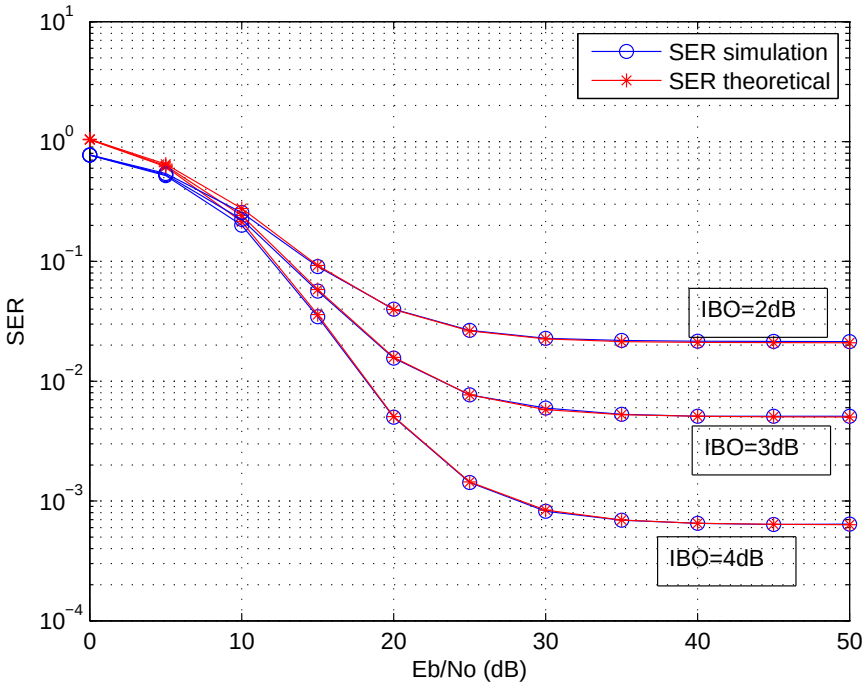

Figure 5-19: WOLA-OFDM performance for different IBOs for HPA2.

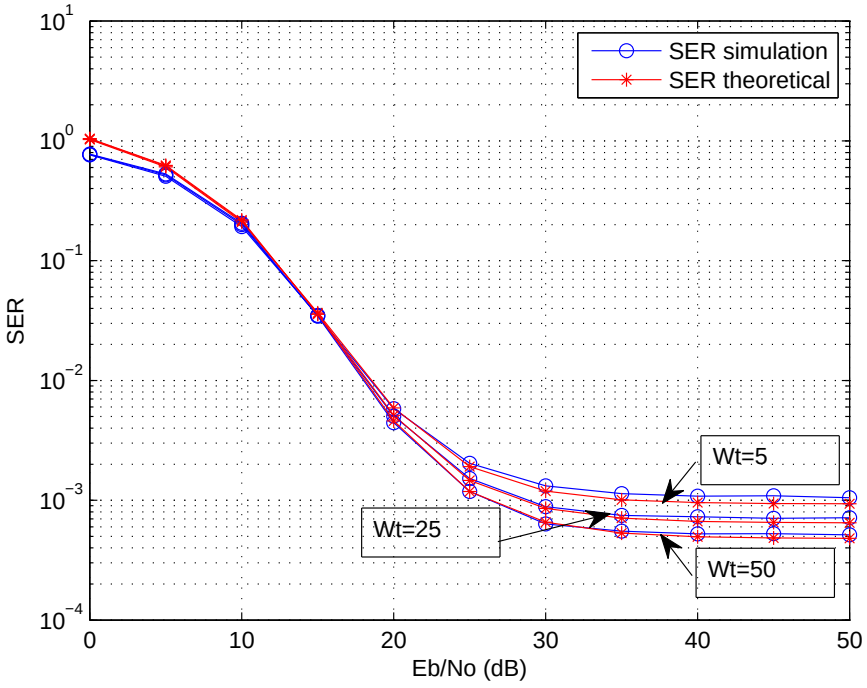

Figure 5-20: WOLA-OFDM performance for different values of Wtx, HPA2, IBO=4dB, Mfft=1024, CP=256, Wtx=[50, 25, 5].

1. $c(0) = h(0)s(0)$
2. $c(1) = h(0)s(1) + h(1)s(0)$
3. $c(2) = h(0)s(2) + h(1)s(1) + h(2)s(0)$
4. $c(n) = \sum_{k=0}^{Lg-1} h(k)s(k-n)$
5. $E(c(n)c(n)^*) = \sum_{k=0}^{n} |h(k)|^2 . E(|s(n-k)|^2) = \sum_{k=0}^{n} |h(k)|^2 . P_0$

where $P_0 = E(|s(n)|^2)$ is the mean power of a time domain sample and h(k) is the impulse response of the transmission filter.

1. For the samples in the first region we have: $E(|c(n)|^2) = \sum_{k=0}^{n} |h(k)|^2 P_0$
2. For the samples in the second region we have: $E(|c(n)|^2) = \sum_{k=0}^{Lg-1} |h(k)|^2 P_0$
3. For the samples in the last region we have: $E(|c(n)|^2) = \sum_{k=n-Mfft-CP-Lg}^{Lg-1} |h(k)|^2 P_0$

Finally the mean power of an UFMC symbol is equal to:

$$P_0[(Mfft + CP + 3.Lg) \sum_{k=0}^{Lg-1} h(k)^2 + 2 \sum_{k=0}^{Lg-1} (Lg - k)h(k)^2] \quad (5.25)$$

where P_0 is the mean power per OFDM sample.

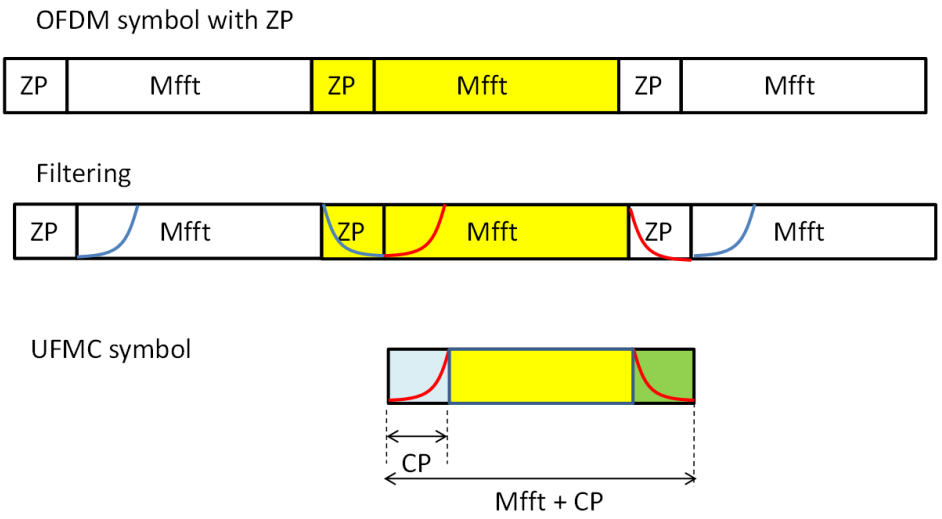

Figure 5-21: UFMC transmitted signal.

The mean power of a UFMC symbol is then lower than the one of OFDM. As for the WOLA case, the UFMC signal has to be amplified in order to have an equivalent IBO as OFDM. This is equivalent to have a lower IBO. Figure 5-22 presents the time domain mean power per sample of a UFMC signal with $Mfft = 1024$, $CP = 72$ and $Lg = 73$. We clearly see on figure 5-22 that, every $(Mfft + CP)$ samples there is a diminution of the mean power due to the filtering effect. The gap between the "'holes"' is equal to $Mfft + CP$ samples.

The gain that has to be applied to the UFMC time domain signal is equal to:

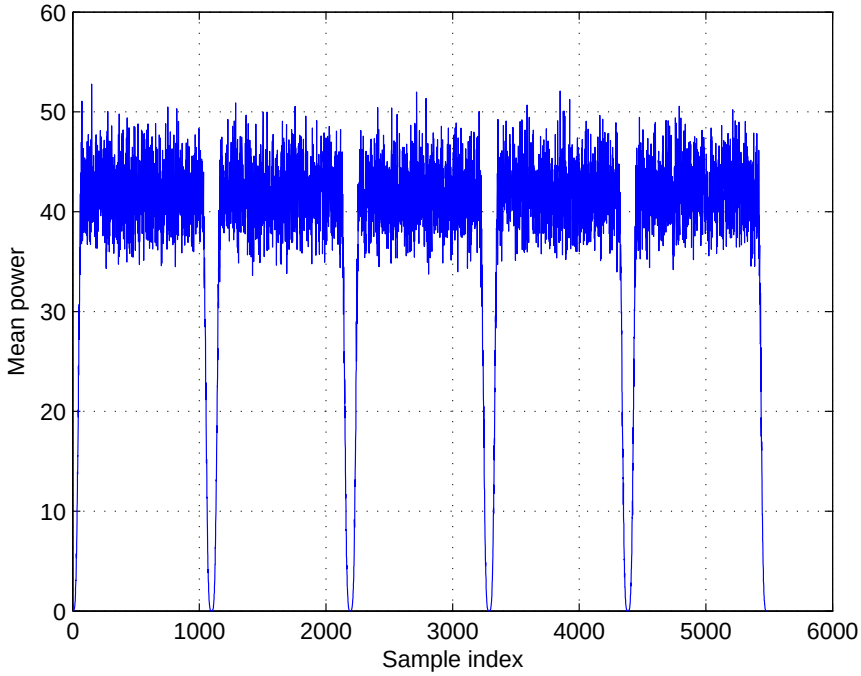

Figure 5-22: UFMC mean power per sample .

$$\Delta_G = \frac{P_0(Mfft + CP)}{P_0(Mfft + CP + 2Lg)\sum_{k=0}^{Lg-1} h(k)^2 + 2\sum_{k=0}^{Lg-k} h(k)^2} \tag{5.26}$$

This extra gain corresponds to an equivalent IBO for UFMC given by:

$$IBO_{UFMC} = IBO_{OFDM} - 10log10(\Delta_G) \tag{5.27}$$

The theoretical SER for UFMC has the same expression as the SER of OFDM except that coefficients K and σ_d^2 are computed for the equivalent IBO_{UFMC} given by equation (5.27).

Figure 5-23 presents the SER of UFMC for $Mfft = 1024$, $CP = 72$, $Lg = CP + 1 = 73$, 64-QAM, for HPA2 with $IBOs = 4, 3, 2dB$. There is a very good match between theoretical expressions and simulation results.

Figure 5-24 presents the SER of UFMC for $Mfft = 1024$, 64-QAM, HPA2 with IBO$= 4dB$ and various values of CP length (36, 72 and 144). When CP is increasing, the width of the holes of figure 8 is increasing, corresponding to a lower equivalent IBO and thus a lower SER performance. We can see on figure 5-24 that there is a good match between theoretical expressions and simulation results.

5.4.3.3 f-OFDM case

As for WOLA and UFMC, we have a signal with a constant mean power on each time domain sample except at the beginning and at the end of the f-OFDM frame. Each $Framelength.(CP + Mfft)$ samples we have a diminution of the samples power due to the filtering at the transmitter side. The filtering and truncation process is presented on figure 5-15. If the number of OFDM symbols per f-OFDM frame (Framelength) is large,

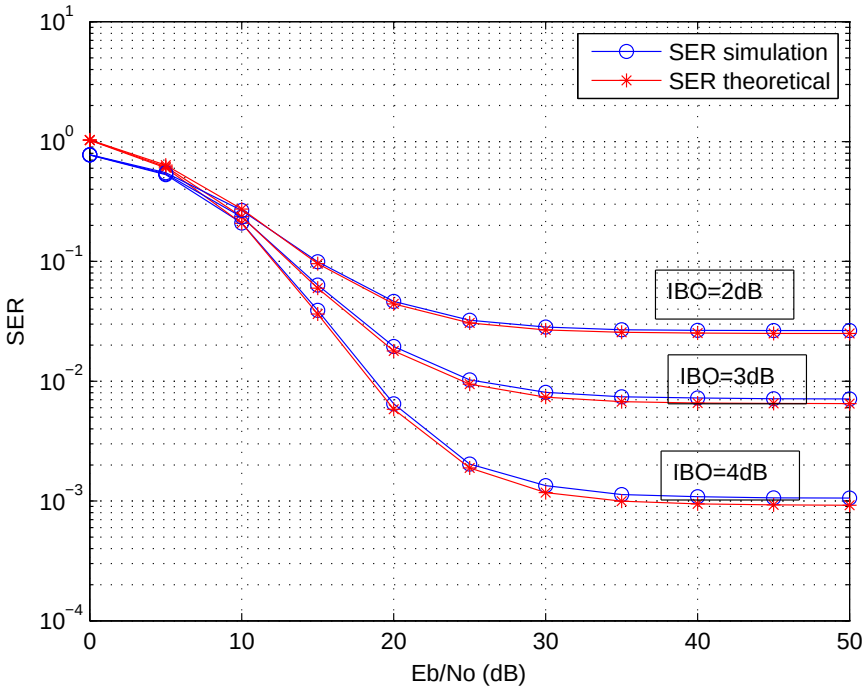

Figure 5-23: UFMC performance for HPA2and IBO=4, 3, 2dB.

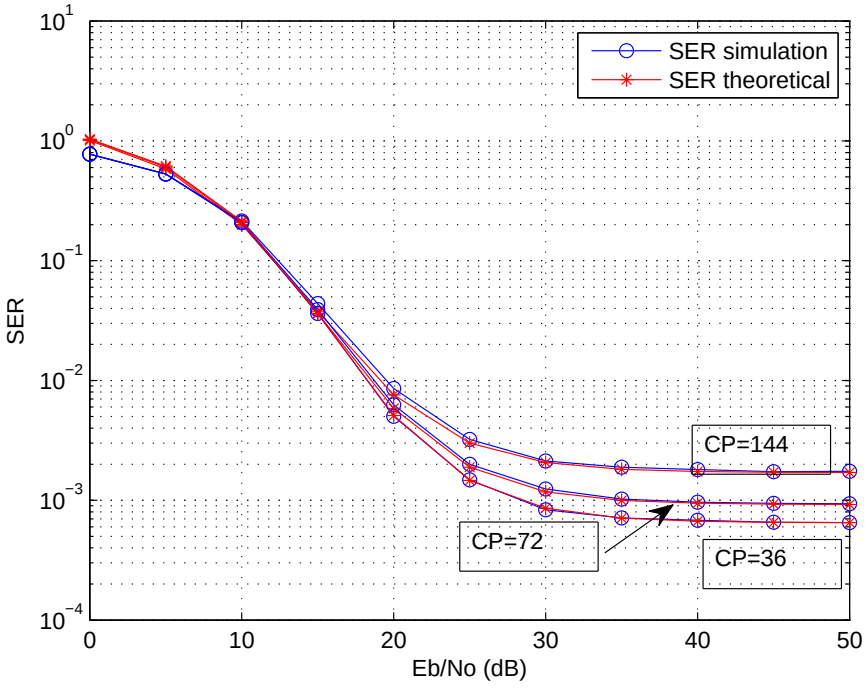

Figure 5-24: UFMC performance for different values of CP length, HPA2, IBO=4dB, Mfft=1024, CP=[36, 72, 144].

the distance between two "'holes"' will be large and the performance will be close to the one of OFDM. Nevertheless, if the number of OFDM symbols per f-OFDM frame is equal to one, there will be a penalty in SER performance. Figure 5-25 presents a single f-OFDM frame.

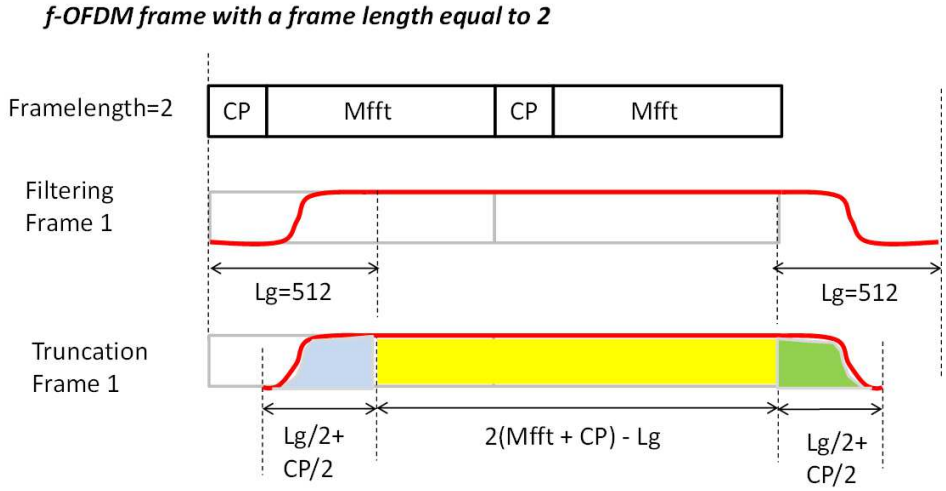

Figure 5-25: f-OFDM symbol.

In figure 5-25, we see that there are three regions in a f-OFDM frame:

- from time domain samples $k = 0 : Lg/2 + CP/2 - 1$ (blue part of f-OFDM frame, figure 5-25).
- from time domain sample $k = Lg/2+CP/2 : Lg/2+CP/2+Framelength(Mfft+CP) - Lg$ (yellow part of of f-OFDM frame, figure 5-25).
- from time domain samples $k = Framelength(Mfft + CP) + CP - Lg/2 - CP/2 : Framelength.(Mfft + CP) + CP$ (green part of f-OFDM frame, figure 5-25).

where Lg is the impulse response filter length ($Lg = 512$).

Because the impulse response is even, mean power per sample in the first region is identical to the one of the samples in the third region.

For the samples in the "'hole"' (first region in blue in figure 5-25) we have:

$$E(|c(n)|^2) = \sum_{k=n}^{Lg-1} |h(k)|^2 P_0 \tag{5.28}$$

where $(n = 0 : Lg/2 + CP/2 - 1)$

For the samples between two "'holes"' (second region in yellow in figure 5-25) we have:

$$E(|c(n)|^2) = \sum_{k=0}^{Lg-1} |h(k)|^2 P_0 \tag{5.29}$$

where P_0 is the mean power per OFDM sample, Lg is the total filter length ($Lg = 512$), $CP = 72$ and $h(k)$ is the impulse response of the filter..

Finally the mean power of an f-OFDM frame is equal to:

$$P_{fOFDM} = P_0.[\sum_{k=n}^{Lg-1} |h(k)|^2 (Framelength(Mfft + CP)Lg) + 2(\sum_{n=0}^{Lg/2+CP/2-1} \sum_{k=n}^{Lg-1} |h(k)|^2)] \tag{5.30}$$

The gain that has to be applied to the f-OFDM time domain signal is equal to:

$$\Delta_G = Po.[Framelength.(Mfft + CP) + CP]/P_{fOFDM} \quad (5.31)$$

This extra gain corresponds to an equivalent IBO for UFMC given by:

$$IBO_{fOFDM} = IBO_{OFDM} - 10log10(\Delta_G) \quad (5.32)$$

The theoretical SER for f-OFDM has the same expression as the SER of OFDM except that coefficients K and σ_d^2 are computed for the equivalent IBO_{fOFDM} given by 5.32.

Figure 5-26 presents the time domain mean power per sample of a f-OFDM signal with $Mfft = 1024$, $CP = 72$, $Lg = 512$ an $framelength = 1$. We clearly see on figure 5-26 that, every $[Framelength.(Mfft + CP) + CP]$ samples there is a diminution of the mean power due to the filtering effect.

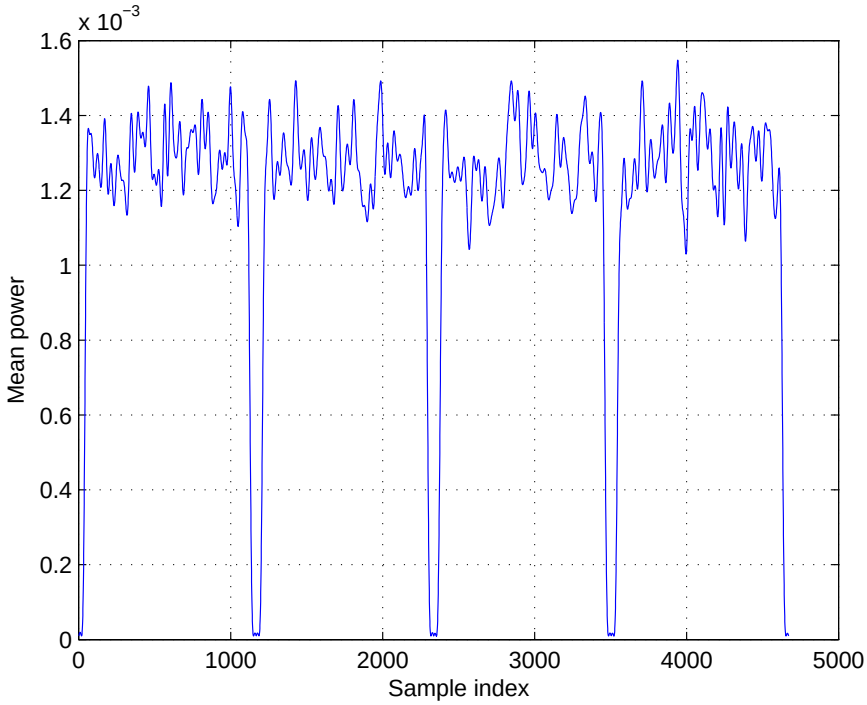

Figure 5-26: f-OFDM mean power per sample

Figure 5-27 presents the SER of f-OFDM for $Mfft = 1024$, $CP = 72$, $Lg = 512$, 64-QAM, for HPA2 with IBOs$= 4, 3, 2dB$. Frame length is equal to one and the number of active subcarriers is equal to $Mfft.31/32 = 992$. There is a very good match between theoretical expressions and simulation results.

Figure 5-28 presents the SER of f-OFDM for $Mfft = 1024$, HPA2 with IBO$= 5dB$, 64-QAM and various values of Frame lengths (1 and 10). When frame length is decreasing, the distance between two holes of figure 5-26 is decreasing, corresponding to a lower equivalent IBO and thus a lower SER performance. We can see on figure 5-28 that there is a good match between theoretical expressions and simulation results.

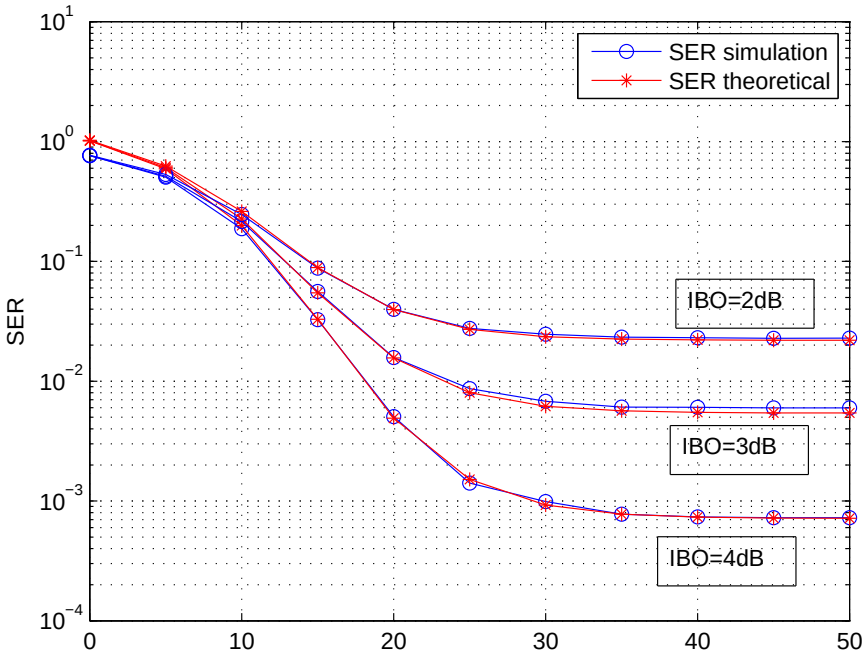

Figure 5-27: f-OFDM performance for HPA2and IBO=4, 3, 2dB.

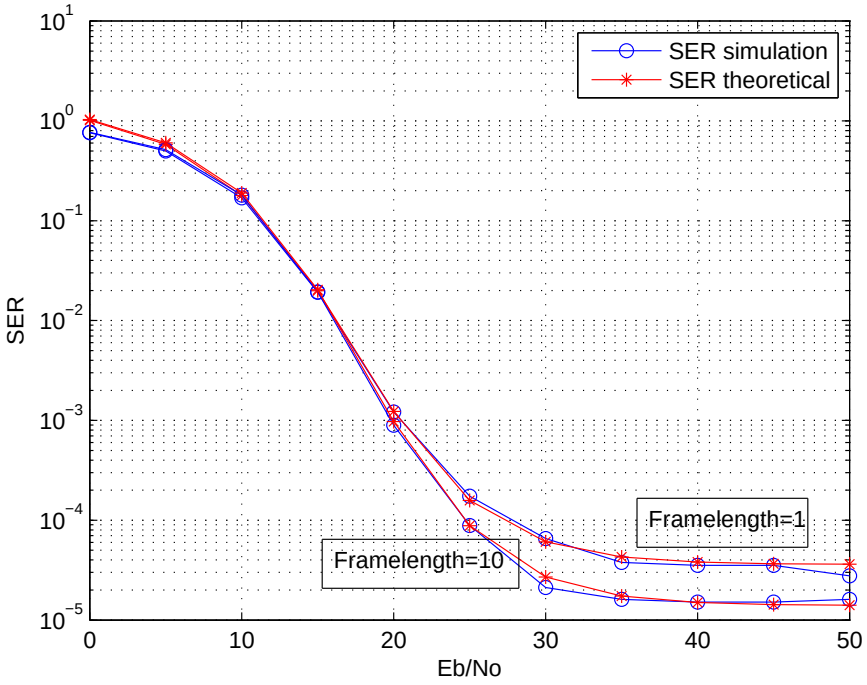

Figure 5-28: f-OFDM performance for different values of frame length (1 and 10), HPA2, IBO=5dB, Mfft=1024, CP=72, Lg=512.

5.4.3.4 SER performance comparison between all WFs

Figure 5-29 presents the SER of all the WFs for the Rapp modified model HPA (HPA2) with an IBO equal to $4dB$ and a 64QAM modulation. Parameters of all WFs are indicated on the figure. FBMC-OQAM and OFDM have the same performance. WOLA, UFMC and f-OFDM have lower performances than OFDM as explained before.

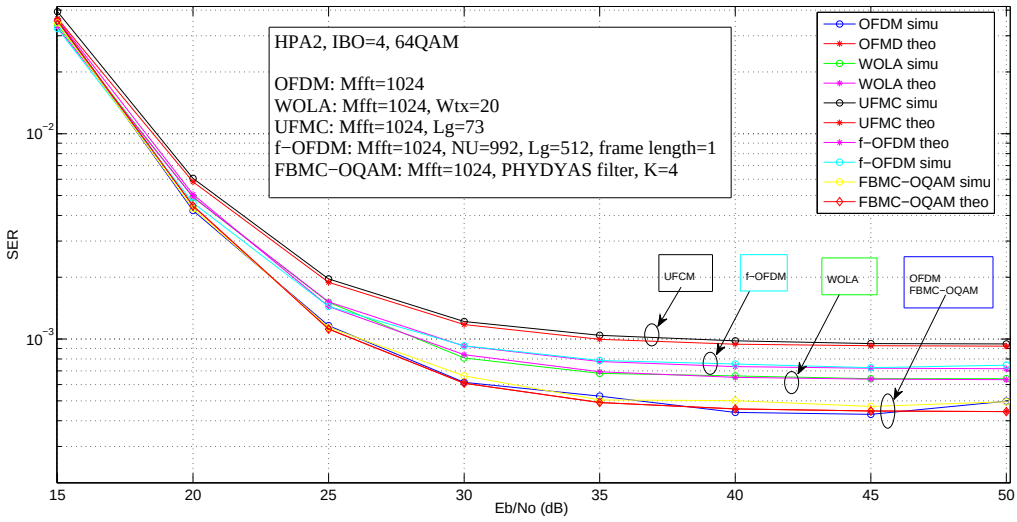

Figure 5-29: SER performance of all WFs for HPA2, IBO=4dB, 64QAM.

Figure 5-30 presents the SER of all the WFs for the 3GPP model HPA (HPA1) with an IBO equal to $4dB$ and a 16QAM modulation. With this HPA we have both AM/AM and AM/PM distortion. Parameters of all WFs are indicated on the figure. As in the case of HPA2, FBMC-OQAM and OFDM have the same performance. WOLA, UFMC and f-OFDM have lower performances than OFDM as explained before.

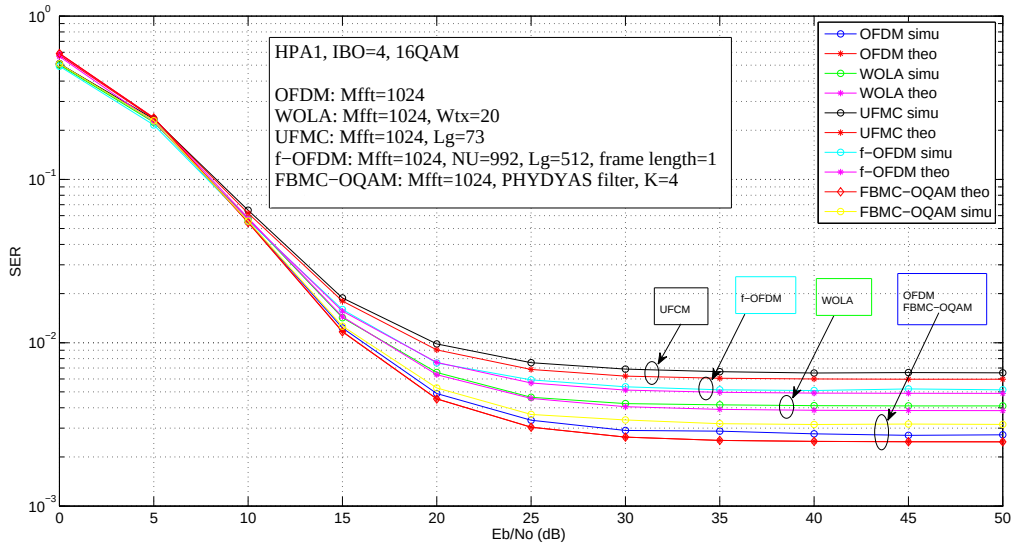

Figure 5-30: SER performance of all WFs for HPA1, IBO=4dB, 16QAM.

5.5 Comparative study of potential waveforms in presence of HPA nonlinearity

In order to offer an objective comparison of the studied waveforms performance in presence of HPA nonlinearity, we present a comparison overview of waveforms performances using two principal criteria NPR gain and SER.

- NPR gain: We consider the NPR measured in the band of the user of interest (540 kHz equivalent to 3 LTE resource blocks) and caused by nonlinearly amplified adjacent users signals. The gain in dB of each waveforms compared to CP-OFDM is considered. The two studied PA models (HPA1 and HPA2) have been considered with two values of IBO ($1dB$ and $4dB$).
- SER: We consider here the in band distortions caused by the HPA. In this case all the sub-carriers are considered as band of interest. Two modulation orders ($16-QAM$ and $64-QAM$) have been considered in presence of the two HPA models considered in this study.

To well present this comparison overview, figure 5-31 shows radar plots where each corner corresponds to a given criteria. A radar plot for each criterion is presented in in order to provide more explanation in the comparison overview.

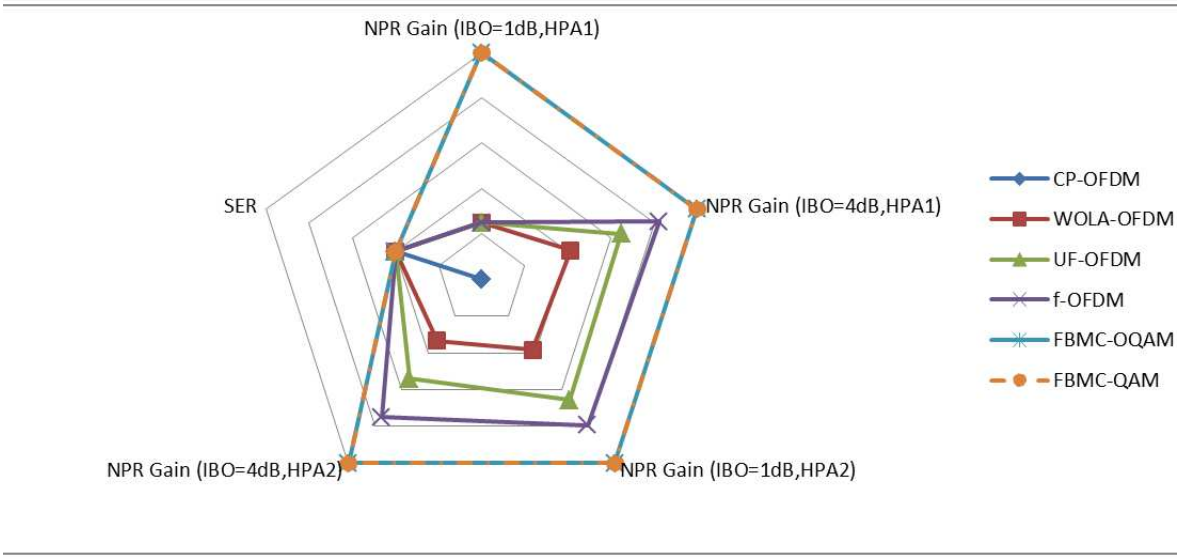

Figure 5-31: Waveforms performances overview in presence of PA nonlinearity.

From the results shown by figures 5-31 and 5-32, we can easily note that all the waveforms, selected in D2.1, are affected by HPA nonlinearities. They offer almost the same SER performance while we note some differences in term of NPR. Indeed, FBMC-QAM and FBMC-OQAM seems to have the lower NPR compared to other waveforms. This is due to the good frequency selectivity of their corresponding filters.

Figure 5-32: Comparison of waveforms performances .

6. Conclusion

In this deliverable D3.1, we aim to analyze the performances of some post-OFDM waveforms in presence of nonlinear power amplifier. All waveforms studied in D2.1 have been considered and compared, analytically and/or by simulations, in terms of PAPR, PSD, NPR and SER. Two models of HPA have been considered in this deliverable :

- (HPA1) : corresponds to the 3GPPP model [RRy16], which is a polynomial model, exhibiting both AM/AM and AM/PM distortions.
- (HPA2) : corresponds to a Rapp model exhibiting only AM/AM distortions, which linear gain was adjusted to reach that of the HPA1 model.

It is well known that PAPR is one of the most detrimental aspects in multicarrier waveforms. As the PAPR of a MCM signal is high, it becomes more sensitive to HPA nonlinearities and generating then in band and out of band distortions. In this deliverable, we provided a theoretical analysis of the PAPR considering all the studied waveforms. From this study, we noted that all multicarrier waveforms have almost the same PAPR even the ones using good frequency selective filters. Despite the good performances provided by these post-OFDM waveforms in terms of robustness to asynchronous transmission and low out-of-band emissions, they present a very important PAPR making them very sensitive to the HPA nonlinearities.

Therefore, an exhaustive and objective study of the impact of HPA nonlinearity on the performance of all the studied waveforms has been done, in this deliverable. We were focused, in one hand, on the out of band distortion where we studied the PSD level in a very large spectral distance and the NPR measured in a spectral notch. In another hand, we analyzed the in band distortion by evaluating the SER where analytical expressions have been introduced for most of the studied waveforms.

From simulations and analytical studies, we noticed that, in presence of a nonlinear HPA, the performances of all the studied waveforms were affected. They lose rapidly the advantages discussed in the perfect linear case. Consequently, the PSD tails become higher and all waveforms have almost the same PSD with severe HPA nonlinearity when the energy efficiency is well optimized (IBO=$0dB$). As the IBO increases, the filtered waveforms provides more robustness to the HPA out of band distortion, a result that was established in the linear case. A high degradation of the SER is also noted for all waveforms. Even if we see some difference between some waveforms compared to others, in terms of SER, this difference is negligible. The study carried in this deliverable brings us to seriously study new techniques for correcting and compensating for the NL effects induced by the HPA. Additionally, special care should be done to reduce the PAPR of MCM signal before amplification, leading then to a system where the trade-off between linearity and energy efficiency is well optimized. Such characteristic is of prime importance in C-MTC context.

7. References

[BC11] H. Bogucka and A. Conti. Degrees of freedom for energy savings in practical adaptive wireless systems. *IEEE Communications Magazine*, 49(6):38–45, Jun. 2011.

[BSR+14] H. Bouhadda, H. Shaiek, D. Roviras, R. Zayani, Y. Medjahdi, and R. Bouallegue. Theoretical analysis of BER performance of nonlinearly amplified FBMC/OQAM and OFDM signals. *EURASIP Journal on Advances in Signal Processing*, doi:10.1186/1687-6180-2014-60 2014.

[CGL09] P. Colantonio, F. Giannini, and E. Limiti. *High efficiency* RF *and microwave solid state power amplifiers*. J. Wiley, UK, 2009.

[CPG14] Marwa Chafii, Jacques Palicot, and Rémi Gribonval. Closed-form approximations of the peak-to-average power ratio distribution for multi-carrier modulation and their applications. *EURASIP Journal on Advances in Signal Processing*, 2014(01), 2014.

[CPGB16] Marwa Chafii, Jacques Palicot, Rémi Gribonval, and Faouzi Bader. A necessary condition for waveforms with better papr than ofdm. *IEEE Transactions on Communications*, 64(08):3395–3405, 2016.

[DTV00] D. Dardari, V. Tralli, and A. Vaccari. A theoretical characterization of nonlinear distortion effects in OFDM systems. *IEEE transactions on Communications*, 48(10):1755–1764, October 2000.

[Lar98] L. E. Larson. Radio frequency integrated circuit technology for lowpower wireless communications. *IEEE Personal Communications Magazine*, 5:11–19, Jun. 1998.

[R4-16] R4-163314. Realistic power amplifier model for the new radio evaluation. In *3GPP TSG-RAN WG4 Meeting No. 79*, pages FS NR newRAT–Release 14. 3GPP, 2016.

[Rap91] C. Rapp. Effects of hpa nonlinearity on 4-dpsk-ofdm signal for digital sound broadcasting systems. *2nd European Conference on Satellite Communications*, pages 38–45, Oct. 1991.

[RQZ04] R. Raich, H. Qian, and G.T. Zhou. Orthogonal polynomials for power amplifier modeling and predistorter design. *IEEE transactions on Vehicular Technologies*, 53:1468–1479, September 2004.

[RRy16] R1-166004(R4-164542)y. *P3GPP TSG-RAN WG1 Meeting No. 85 R1-166004*. Nanjing, China, 2016.

[Sal81] A. A. Saleh. Frequency-independent and frequency-dependent nonlinear models of twt amplifiers. *IEEE Transactions on Communications*, 29(11):1715–1720, Nov. 1981.

[SM98] D. Su and W. McFarland. An ic for linearizing rf power amplifiers using envelope elimination and restoration. *ISSCC Digest of Technical Papers*, 22(12):54–55, Dec. 1998.

[YKK+15] Yeo Hun Yun, Chanhong Kim, Kyeongyeon Kim, Zuleita Ho, Byunghwan Lee, and Ji-Yun Seol. A new waveform enabling enhanced qam-fbmc systems. In *Signal Processing Advances in Wireless Communications (SPAWC), 2015 IEEE 16th International Workshop on*, pages 116–120. IEEE, 2015.

[ZBR08] R. Zayani, R. Bouallegue, and D. Roviras. Adaptive predistortions based on neural networks associated with levenberg-marquardt algorithm for satellite down links. *EURASIP Journal on Wireless Communications and Networking*, 2008(132729), 2008.

[ZK01] G. T. Zhou and J. Stevenson Kenney. *Predicting spectral regrowth of nonlinear power amplifiers*. Georgia Institute of Technology, 2001.

[ZR04] G. T. Zhou and R. Raich. Spectral analysis of polynomial nonlinearity with applications to rf power amplifiers. *EURASIP Journal on Applied Signal Processing*, 2004(256395):1931–1840, 2004.

Glossary and Definitions

Acronym	Meaning
AM/AM	amplitude to amplitude
AM/PM	amplitude to phase
BER	Bit Error Rate
C-MTC	Critical-Machine Type Communications
COQAM	Circular Offset QAM
CP	Cyclic Prefix
CCDF	Complementary Cumulative Distribution Function
EVM	Error Vector Magnitude
FBMC	Filter Bank Multi-Carrier
f-OFDM	filtered-OFDM
GWMC	Generalized Waveforms for MultiCarrier
HPA	High Power Amplifier
IB	In Band
IBO	Input Back-Off
MCM	Multi Carrier Modulation
MGF	Moment-Generating Function
NL	non-linear
NPR	Notch Power Ratio
OFDM	Orthogonal Frequency Division Multiplexing
OOB	Out Off Band
PAPR	Peak to Average Power Ratio
PSD	Power Spectral Density
RB	Resource Block
SEL	Soft Envelope Limiter
SER	Symbol Error Rate
SSPA	Solid State Power Amplifiers
TWTA	Travelling Wave Tube Amplifiers
UFMC	Universal-Filtered Multi-Carrier (i.e. Universal-Filtered OFDM)
WF	WaveForm
WOLA	Weighted Overlap and Add